Advanced Materials Intelligent Processing Center

Phase VI

DISTRIBUTION STATEMENT A
Approved for Public Release
Distribution Unlimited

FINAL REPORT

May 12, 2004-December 31, 2005

ONR Grant Number N00014-04-1-0574
Principal Investigators:
Professor Suresh G. Advani and
Professor J .W. Gillespie, Jr.
Program Officer: Mr. Ignacio Perez

Submitted to ONR: April 4, 2006
University of Delaware
Center for Composite Materials

REPORT DOCUMENTATION PAGE

OMB No. 0704-0188

1. REPORT DATE (DD-MM-YYYY)	2. REPORT TYPE	3. DATES COVERED (From - To)
4-04-2006	Final Technical Report	May 12 2004 - Dec 31 2005

4. TITLE AND SUBTITLE
Advanced Materials Intelligent Processing Center: Materials For Intelligent [illegible]

5a. CONTRACT NUMBER

5b. GRANT NUMBER
[illegible]

5c. PROGRAM ELEMENT NUMBER

6. AUTHOR(S)
Advani, Suresh, G, and Gillespie, John, W, Jr.

5d. PROJECT NUMBER

5e. TASK NUMBER

5f. WORK UNIT NUMBER

7. PERFORMING ORGANIZATION NAME(S) AND ADDRESS(ES)

Center for Composite
Materials
University of Delaware
Newark, DE 19716

8. PERFORMING ORGANIZATION REPORT NUMBER

9. SPONSORING / MONITORING AGENCY NAME(S) AND ADDRESS(ES)

Office of Naval Research
100 Alabama Street, SW
Suite 4R15
Atlanta, GA 30303-3104

10. SPONSOR/MONITOR'S ACRONYM(S)
ONR

11. SPONSOR/MONITOR'S REPORT NUMBER(S)

12. DISTRIBUTION / AVAILABILITY STATEMENT

Approved for public release

13. SUPPLEMENTARY NOTES

14. ABSTRACT

The work performed by the University of Delaware Center for Composite Materials builds on previous ONR-funded phases of the Advanced Materials Intelligent Processing Center (AMIPC). This work continues the establishment of 21st Century manufacturing practices using intelligent processing to accelerate the insertion of composites into ship applications. Quality, repeatability, tolerances, and affordability can be improved through computer simulations and process design tools as well as automation combining advanced sensors and process control.

The overall goal is to develop and use sensors, science-based simulations, and process control to advance composite manufacturing with Liquid Composite Molding Processes. Advanced sensors have been developed and validated in a manufacturing environment. Simulations incorporate resin impregnation and cure physics occurring at micro, meso, and macro levels during manufacturing. Passive and active feedback control strategies(continued)

15. SUBJECT TERMS
Composite materials, Processing, Control, Resin transfer molding, Vacuum-assisted resin transfer molding, simulation, sensors

16. SECURITY CLASSIFICATION OF:			17. LIMITATION OF ABSTRACT	18. NUMBER OF PAGES	19a. NAME OF RESPONSIBLE PERSON
a. REPORT	b. ABSTRACT	c. THIS PAGE			John W. Gillespie Jr., Director
U	U	U	UU	56	19b. TELEPHONE NUMBER (include area code) (302) 831-8702

have been formulated to improve process control. Automation of the process to reduce labor and improve yield has been attempted. Technology transfer has been accelerated by creating user friendly software and hardware interfaces to implement the methodologies in the manufacturing platform.

management using advanced photonics and left handed materials. Meeting these requirements involves processing of multiple resins encapsulating different inserts with possible interconnections for power supply, creating the next generation of composite structures. The program tasks address the intelligent processing aspect with the goal of addressing multifunctional design, followed by assessment projects to explore multifunctional attributes of composites.

The framework of intelligent processing has been advanced through the development and use of Resin Transfer Molding (RTM) and Vacuum Assisted Resin Transfer Molding (VARTM) to address processing, sensing, and control methodologies. The program tasks have included (i) Process physics and simulation in which we focused on the physics of fabric compression and simulation challenges for multifunctional parts, role of surface tension and wetting when embedding devices in the structure and new process developments containing loaded resins and use of membranes as vents (ii) Design and optimization focused on approaches to create a blueprint of the distribution media network to successfully infuse resin despite the presence of inserts and devices in the composite, build new actuation mechanisms to redirect the resin and also characterize the variability of the process so it could be accounted for i n design and control of the process (iii) Sensing, control and inspection continued the development of the TDR sensor and vibrational techniques for applications in structures containing embedded devices and (iv) Validation and implementation integrated all the above in a test bed and demonstrate the combined usefulness of all the tools to move towards repeatability and affordability. Two new projects to specifically address issues for multifunctional composites were pursued. The first one explored seamless integration of conformal antenna arrays into a composite structure with complex curvatures. Due to the growing interest in blast-resistant naval structures, the second new initiative investigated many innovative material concepts including cellular materials of different kinds in composite structures and characterized methods for energy absorption.

The researchers selected a test-bed of tall structures to validate the processes and all the methodologies developed in the program. The program has independently tested the sensors developed, process models and simulations, low-cost resin behavior, optimization techniques for gate, vent, sensor, and distribution media locations, control strategies, injection systems, and software to transfer the methodology from the virtual simulation environment to the manufacturing platform, validated inspection and health monitoring systems, and explored user-friendliness and technology readiness by transitioning it to an industrial environment. These technologies have been and will continue to be transitioned to Navy labs, shipyards, and the industrial base as part of this program.

Contract Information

Contract Number	N00014-04-1-0574
Title of Research	Advanced Materials Intelligent Processing Center: Materials for Multi-functionality
Principal Investigators	John W. Gillespie, Jr. and Suresh G. Advani
Organization	University of Delaware Center of Composite Materials

Technical Section

Technical Objectives

The work being performed by the University of Delaware Center for Composite Materials builds on previous ONR-funded phases of the Advanced Materials Intelligent Processing Center (AMIPC). This work continues the establishment of 21st Century manufacturing practices using intelligent processing to accelerate the insertion of composites into ship applications. Quality, repeatability, tolerances, and affordability can be improved through computer simulations and process design tools as well as automation combining advanced sensors and process control.
The overall goal is to develop and use sensors, science-based simulations, and process control to advance composite manufacturing with Liquid Composite Molding Processes. Advanced sensors have been developed and validated in a manufacturing environment. Simulations incorporate resin impregnation and cure physics occurring at micro, meso, and macro levels during manufacturing. Passive and active feedback control strategies have been formulated to improve process control. Automation of the process to reduce labor and improve yield has been attempted. Technology transfer has been accelerated by creating user-friendly software and hardware interfaces to implement the methodology on the manufacturing platform.
This suite of software and hardware tools developed in the previous phases has been used and expanded to address the needs of the Navy for revolutionary multifunctional composite materials. Multi-functionality requirements arise from various needs, such as fire protection, blast resistance, and embedded antennas as well as signature management using advanced photonics and left-handed materials. Meeting these requirements involves processing of multiple resins encapsulating different inserts with possible interconnections for power supply, creating the next generation of composite structures. The program tasks address the intelligent processing aspect with the goal of addressing multifunctional design, followed by assessment projects to explore multifunctional attributes of composites.

The framework of intelligent processing has been advanced through the development and use of Resin Transfer Molding (RTM) and Vacuum Assisted Resin Transfer Molding (VARTM) to address processing, sensing, and control methodologies. The program tasks have included (i) Process physics and simulation in which we focused on the physics of fabric compression and simulation challenges for multifunctional parts, role of surface tension and wetting when embedding devices in the structure and new process developments containing loaded resins and use of membranes as vents (ii) Design and optimization focused on approaches to create a blueprint of the distribution media network to successfully infuse resin despite the presence of inserts and devices in the composite, build new actuation mechanisms to redirect the resin and also characterize the variability of the process so it could be accounted for in design and control of the process (iii) Sensing, control and inspection continued the development of the TDR sensor and vibrational techniques for applications in structures containing embedded devices and (iv) Validation and implementation integrated all the above in a test bed and demonstrate the combined usefulness of all the tools to move towards repeatability and affordability. Two new projects to specifically address issues for multifunctional composites were pursued. The first one explored seamless integration of conformal antenna arrays into a composite structure with complex curvatures. Due to the growing interest in blast-resistant naval structures, the second new initiative investigated many innovative material concepts including cellular materials of different kinds in composite structures and characterized methods for energy absorption.

The researchers selected a test-bed of tall structures to validate the processes and all the methodologies developed in the program. The program has independently tested the sensors developed, process models and simulations, low-cost resin behavior, optimization techniques

for gate, vent, sensor, and distribution media locations, control strategies, injection systems, and software to transfer the methodology from the virtual simulation environment to the manufacturing platform, validated inspection and health monitoring systems, and explored user-friendliness and technology readiness by transitioning it to an industrial environment. These technologies have been and will continue to be transitioned to Navy labs, shipyards, and the industrial base as part of this program.

Tasks to Advance the Framework of Intelligent Processing

The research in this program has developed and integrated the four pillars shown in Figure 1 that form the framework of intelligent processing to specifically address the manufacturing of non-planar structures containing various inserts and complexity to perform various integrated passive and active functions.

Task 1: Model Enhancements for Vacuum Infusion (VI) Processes

Liquid Composite Molding – Description, Modeling and Simulation

In-depth analysis of two issues, fundamental to further development of the field, was performed and is summarized below.

Essentially, the issue of expanding the process model to fully include "general" LCM process – such as VI, RTM Light or Compression RTM – was undertaken. Currently, the process modeling is still based on analysis performed for the conventional Resin Transfer Molding. However, in other variations of Liquid Composite Molding such as VI process, new issues arise and the influence of some phenomena is much more significant for general VI process than for conventional RTM. Consequently, these phenomena must be included into the model. The modeling issues are:

- The resin flow is fully three-dimensional. The material is highly non-homogenious as distribution media and runners must be modeled. This issue has been already resolved and presents no current problem.
- Preform and distribution media deformation during the flow process. This modifies the governing equations. The change is very significant particularly as there is a coupling between resin pressure and the porous media deformation and this area has been avoided in previous research. We have studied and modeled the preform deformation effect previously, but the existing "solution" is not suitable for practical deployment. To truly resolve this issue, one must incorporate major changes to the existing model.
- With the process pressure limited, fiber tow saturation becomes a significant issue. We already have working numerical models for fiber tow saturation, but material characterization, and verification must be addressed. Also, better integration into process model is sought.
- The effects of gravity field on the resin flow may be significant. This issue has been addressed with some degree of success and we have a numerical implementation for the model with gravity included, but it is not well integrated into modeling capability.

The work undertaken in this period attempted to address the issues listed above. The significant steps undertaken during this period were:

- New governing equations for the flow process were developed. New model is necessary to handle the preform deformation issue. It also allows us to integrate the existing modeling capability for fiber tow saturation and gravity. The new set of governing equations include, apart from resin pressure and fill factor, also the preform deformation and fiber tow saturation as primary unknowns. This inclusion requires incorporation of several constitutive models governing preform deformation and fiber tow saturation.
- The numerical implementation of the above scheme is in progress.

- Experiments were carried out to characterize fiber tow saturation and to compare it with the existing numerical model. The resulting comparison proved successful. The ultimate goal is to develop experiment to provide material data necessary for modeling of the fiber tow saturation.
- Analytic model of fiber-tow saturation was successfully created and compared with numerical results and experimental data
- Gravity term was incorporated into the simulation package LIMS and properly tested

Simulation Software Development and Deployment

- LIMS simulation package was maintained during the period. No significant additions were made, but number of issues was fixed.
- The experimental LIMS version including gravity was successfully tested by comparison to both experiments and analytic solution.
- LimsUI graphical user interface was maintained and significantly enhanced to simplify the user interaction. Also, the options how the simulation is actually executed were enhanced. The program now offers simpler interface and multiple scenarios for simulation end. Several smaller enhancements and bug-fixes were also made. Currently, the use of material database and simplified property handling is being tested.
- The software tools for mesh creation and manipulation were enhanced. Among others, it is now possible to create the cross-section models for thick panels with ply drop-offs and elements aligned with preform layers.
- Modeling support was provided for other groups working on this project as well as for some industrial partners.

Task 2: Microflow and Microvoids around Embedded Objects

Experimental Approach to Validate Analytical Model

An analytical model was proposed to describe the capillary infusion of a liquid (resin) across an array of parallel micro-cylinders (aligned fibers). Based on a series of simplifying assumptions the model can be applied to the case of transverse capillary impregnation of fiber tows, the opposing effect of gas (air) displacement and entrapment being taken into consideration.

The role played by air displacement in the capillary impregnation was modeled by introducing a new parameter δ, describing the rate at which the air dissolves or escapes out of the tow. To determine the rate at which the resin saturates the tow, one must have not only the correct estimation for the tow permeability, but also be able to accurately approximate parameter δ.

Figure 1 shows how the impregnation dynamics and therefore the tow fill time depend on the value of parameter δ. Case $\delta=0$ (no air, or easy air escape outward of the tow) is the most favorable case for the impregnation, which takes place in the shortest time. If $\delta=1$, the air is compressed inside of the tow without any part of the preexisting air emerging. Any other value of δ between zero and one gives a finite impregnation time, always larger than when $\delta=0$.

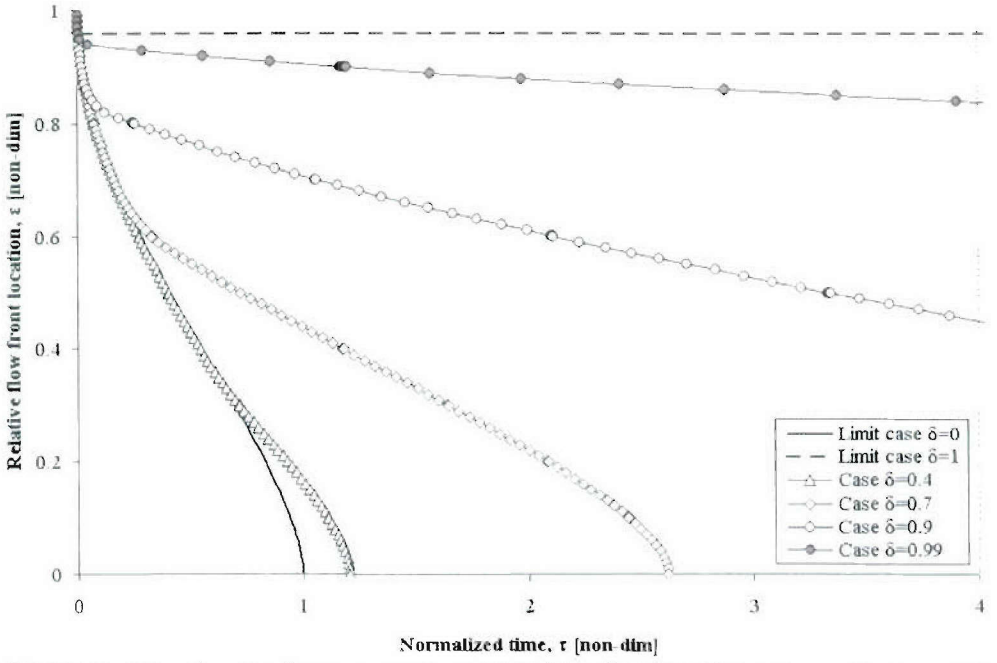

Figure 1. Flowfront advancement versus time, for several values of parameter δ. Both axes are dimensionless.

An experimental approach was aimed at checking the validity of the analytical model and obtaining insight into what are the parameters which affect the air displacement through the tow and consequently the overall tow impregnation and its fill time.

The experimental setup consists of samples devised as enlarged replicas of real fiber tows, inside which hand-made sensors were placed at certain radial locations. A data acquisition system was used to provide a continuous reading of the sensors status, so that the arrival times

of the impregnating resin at the sensor locations were detected (Figure 2). The tests were conducted by immersing the sample in a liquid with no imposed pressure difference to assist the flow. Hence the flow was exclusively driven by the capillary pressure.

The experimental study presented in this paper validated the theoretical model proposed. Capillary impregnation tests conducted on hollow samples simulated the ideal case in which the air could escape without exerting any back pressure ($\delta = 0$). This also verified the equations used to approximate the mean capillary pressure and the transverse permeability.

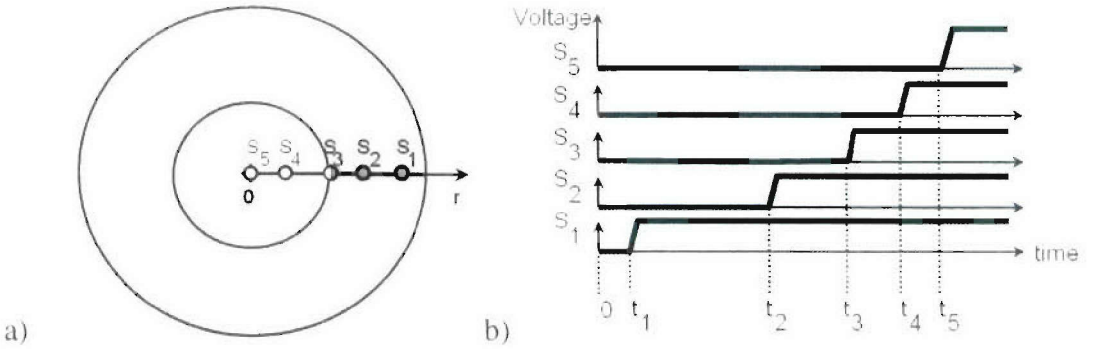

Figure 2. a) Sensors location in radial direction, shown in a cross-sectional view through the mid-plane of a full sample. The grey area corresponds to the already wetted porous medium, whereas white indicates the inside region which is still dry. b) Sketch of the signals read from the sensor circuits by the data acquisition system, which records the arrival times $t_1 - t_5$ at sensors $S_1 - S_5$

Tests conducted on full samples helped better understand the role of air entrapped and its dissolution, on the overall impregnation dynamics. A single parameter, δ was shown to account for the influence of the entrapped air. This parameter also shed light on the influence of external liquid pressure and fiber volume fraction on the ease with which the air could escape.

Among the results, it was shown that there is a direct dependence of parameter δ on fiber volume fraction V_f (see Figure 3). It is remarkable that increasing fiber volume fraction V_f is associated with higher values of parameter δ, which indicate a more inhibiting role of the air escape/dissolution in the capillary impregnation process. The results presented in Figure 3 are for a range of fiber volume fractions from 45 to 70%, for which a quadratic trend was identified, approximated well with a R-squared value of 0.98, as:

$$\delta \approx 0.9945 \cdot V_f^2 + 2.0524 \cdot V_f \qquad (1)$$

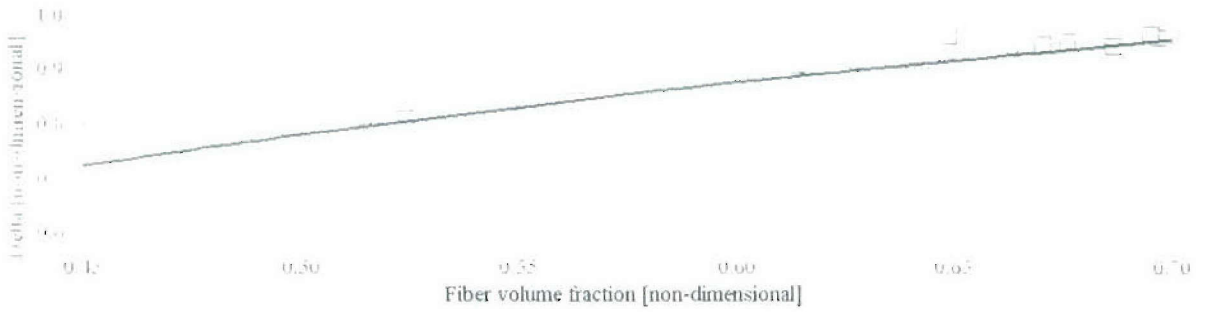

Figure 3 Variation of parameter δ, versus fiber volume fraction V_f. The trend indicate that denser packing (higher V_f) causes higher values of parameter δ, which is equivalent to a more significant role played by the inside air, in opposing the capillary flow.

Our experimental study serves as an illustration that the analytical model can be used to model the capillary impregnation. Thus, one could use the analytical model proposed to simulate the capillary impregnation process, for any arbitrary new case, once the constitutive equation for parameter δ is determined.

Magnetic Resonance Imaging

Magnetic Resonance Imaging (MRI) was also used, as a more powerful experimental technique to better understand the mechanisms of capillary impregnation of fiber tows. The information provided by this technique allows for 2D monitoring of the capillary flow, with a much better time resolution, which allows finding an unambiguous curve fit to a time dependent series of data points. In addition to that, the MRI technique is non-invasive, not disrupting the flow behavior by the presence of sensors. Typical results of a capillary impregnation test are shown in Figure 4.

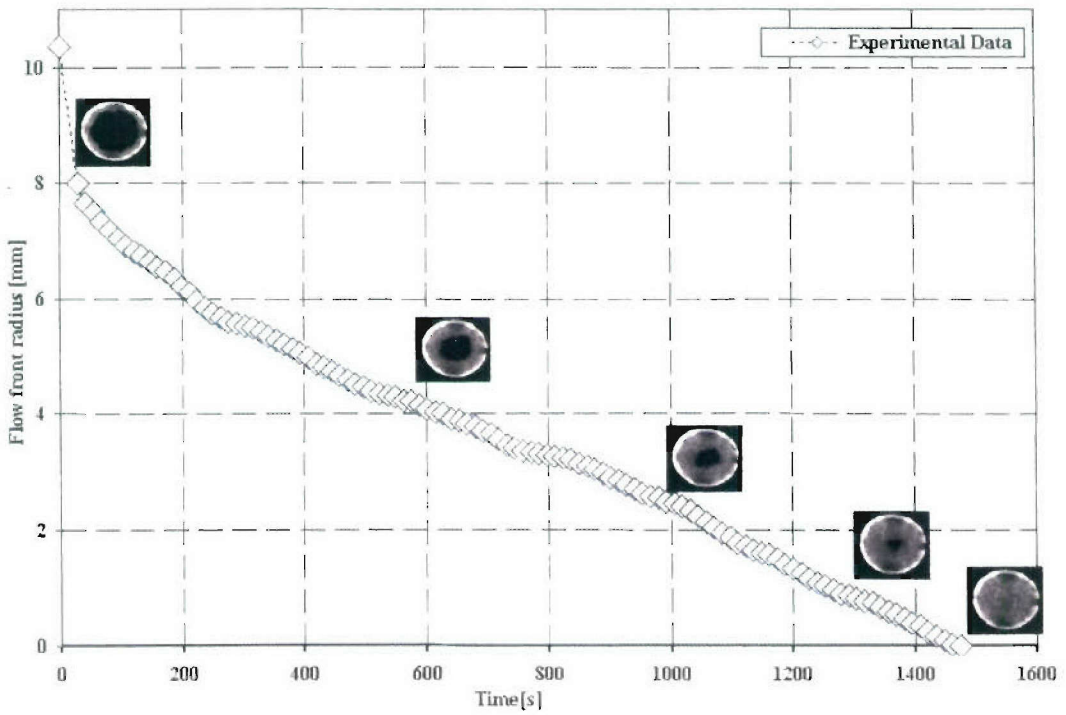

Figure 4 Typical experimental curve of flow front dependence of flow front radius vs. time. Each point corresponds to an image acquired by the spectrometer.

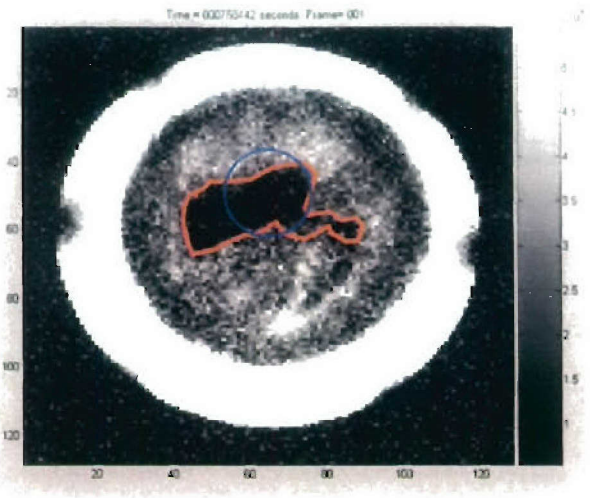

Figure 5 Irregular flow front contour following transverse capillary impregnation in a cylindrical fiber tow. The irregular inner dark area shows the dry fiber, while the light grey region around it is the wet fiber.

Another reason for our pursuing this alternative experimental approach is that MRI can reveal the irregularities of the flow front, which not always keeps the original shape of the cross section of the tow (see Figure 5). A model for quantifying the irregularity of the flow front was also proposed.

MRI permits investigating how various parameters (liquid viscosity and surface tension, fiber material, fiber diameter and sample size) influence the irregularity of the flow front, as well the discrepancy between the real capillary flow behavior and the theoretical one, which would be displayed if air were absent from the sample.

The work on a series of 15 MRI tests is presently in progress; the final results being then compiled into a paper to be submitted for publication.

Task 3: Processing of Functionally Gradient Materials and Multiple Resins

Functionally Graded Composites exhibit properties or functions within the material that vary gradually or in a step-wise manner without a recognizable boundary. One technique to manufacture Functionally Graded Polymer Composites is by a molding process. In this process layers of glass, Kevlar, or carbon fabric are stacked in a closed mold and resin with suspended micron-size particles is injected into the mold. The fabrics are usually yarns or bundles of thousand or more micron-size fibers woven, stitched or knitted together. This architecture gives rise to a bimodal distribution of pore sizes; the larger pores in between the bundles and smaller ones within the bundles. This dual-scale nature of the fabrics create a network of pore sizes through which the resin will flow to cover the fibers but the infiltration and the final concentration distribution of the particles will establish the gradient of the properties in the composite.. In this task we developed a model to predict the concentration distribution of particles within this dual scale fibrous porous media infused under a constant pressure drop. The approach uses Darcy's law and accounts for lowering in the permeability value due to the particle entrapment in the available pores. Experiments are conducted and the concentration of the particles in the fabric is measured. The results compare well with the predictions.

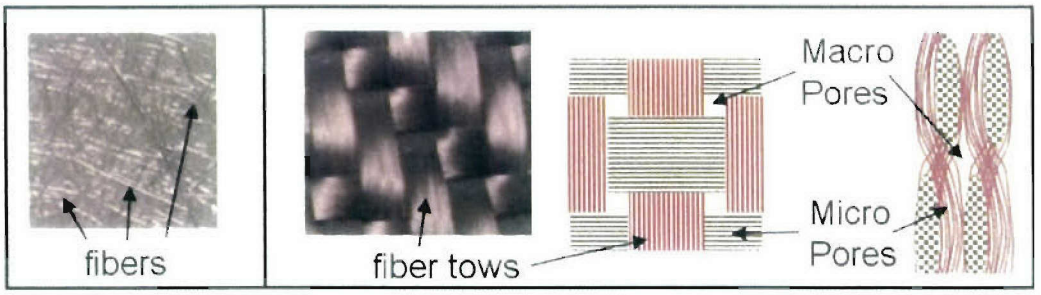

Figure 6 a) left: A preform with single porosity (random mat). b) right: A preform with dual porosity (woven preform).

In classical filtration modeling includes a microscale (of the order of the collector size), and a macroscale, comparable to the filter external size. Because of the dual-scale porosity present in the woven fabrics as shown in Figure 6 above, there is an additional mesoscale which is characterized by the average size of macropores and tows as shown schematically in Figure 7.

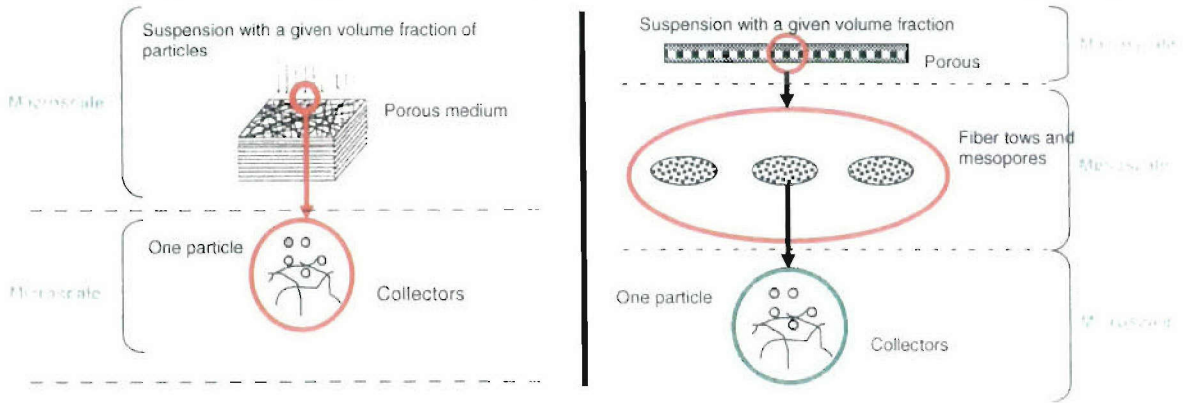

Figure 7 a) left: scales involved in classical filtration. b) right: introduction of a intermediary scale for preforms with dual porosity (woven preform).

This multiscale filtration phenomenon will be a function of material and process parameters and network analysis to flow analogy was used to model this flow as shown schematically in Figure 8.

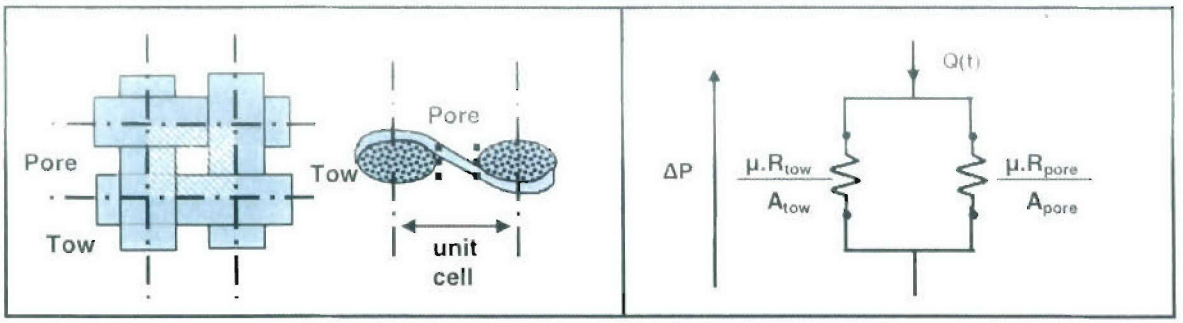

Figure 8 a) left: schematics of the considered unit cell in dual scale porosity preform. b) right: resistance to flow analogy.

Results

The results show an increase of particles deposition with time which becomes less and less significant with time. Indeed, because of the increase of the cake resistance and as the suspension is subjected to a constant pressure drop across the fabric, the flow through the tow region will decrease with time which will result in less particles being trapped in it (Figure 9a). The resistance of the preform can be determined as well from the resistance analogy of a unit cell (Figure 8). We observe an increase of the resistance due to the particles' deposition (Figure 9). However, this increase is negligible as the resistance of the macropores is much smaller and it is constant with respect to time.

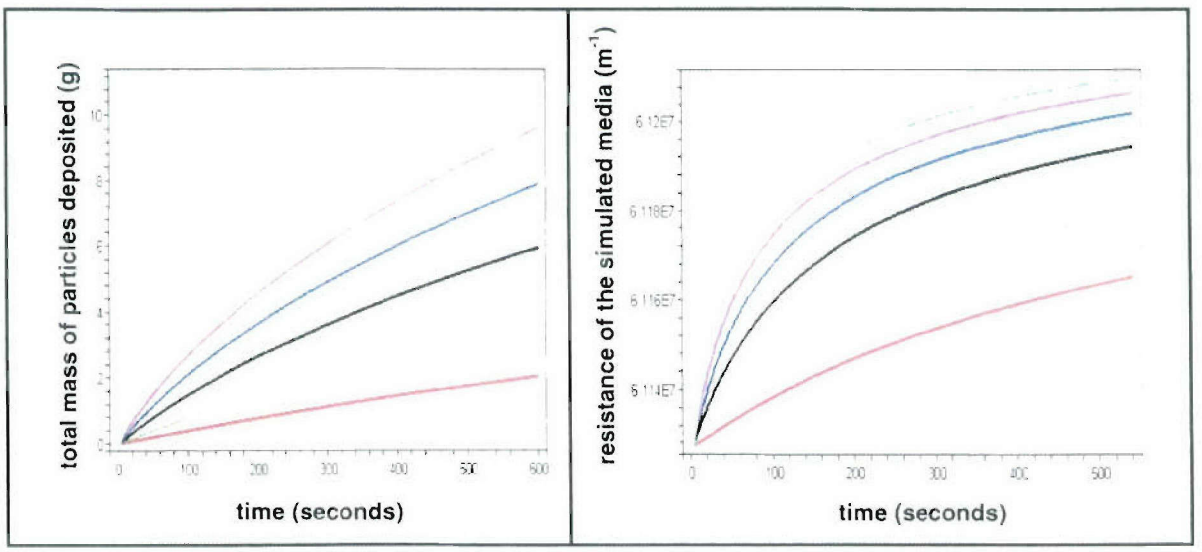

Figure 9 a) left: total mass of particles deposited as a function of time for various particles concentration in the slurry (mass fractions: 1%, 2%, 4%, 6%, 8%, and 10%). b) right: total resistance of the perform and particles as a function of time for the same particles concentration.

Material Parameter Determination

An experimental validation of the model proposed was carried out and is presented here. The preform used was a S-2 Glass 15x15 woven preform for the experiments. Its different characteristics needed for modeling were measured. Because of deformation due to shear especially during cutting operations, pore size distribution may become very random. To avoid that, fibers were cut using a laser, which doesn't affect the pores size and the shape of preforms. The pore size distribution is measured by microscopy and image analysis, through the diffusion of light through the preform. Then the light spots were measured to determine the different dimensions needed as shown in Figure 10.

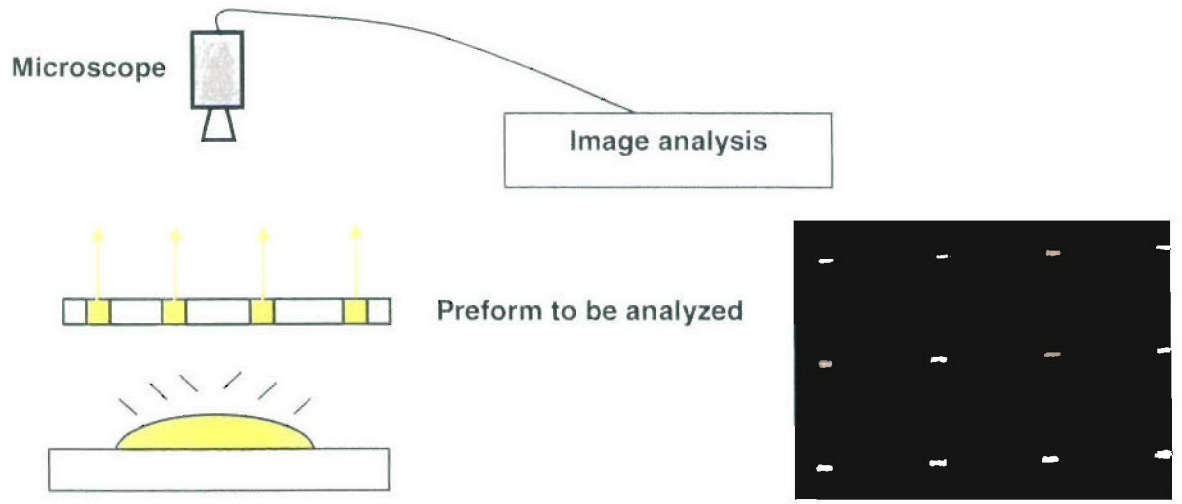

Figure 10 Determination of the pore area distribution using image analysis. The macropores allow the light to pass and the illuminated area is calculated.

Using the same approach, the area of the tow region for average unit cell is measured through microscopy and image analysis.

Suspension Preparation

An experimental setup was designed to obtain repeatable results and to avoid the effects of disturbances that naturally occur during filtration experiments. During the particles transport, particles do have a tendency to form aggregates. This will make the particle concentration non-uniform and violate the assumption in our model. To promote uniformity, we used an online static mixer to shear and break any aggregates in the incoming suspension. The mixing also ensured that the concentration was uniform before infusion.

To continuously evaluate and maintain the incoming concentration of the particles in the suspension, an inline measurement and PID controlled mixing station was used to ensure constant mixing ratio between particles and fluid through the use of a computer controlled peristaltic pump, as shown in Figure 11. The static mixer in-line ensured that the concentration was uniform before it infiltrated the fiber preform.

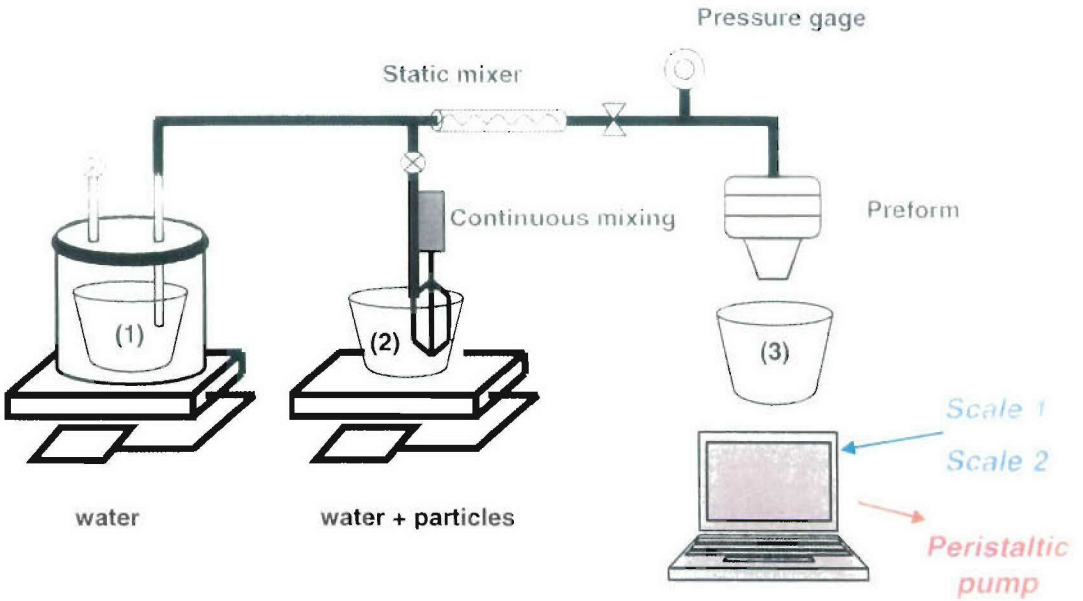

Figure 11 Experimental setup used for the filtration experiments.

Experimental Results

The slurry concentrations were determined using the mix inline station and input in the algorithm. For different concentration profiles, we obtained results which correlated quite well with the model's results for mass of particles deposited, as well as resistance of the preform to the flow.

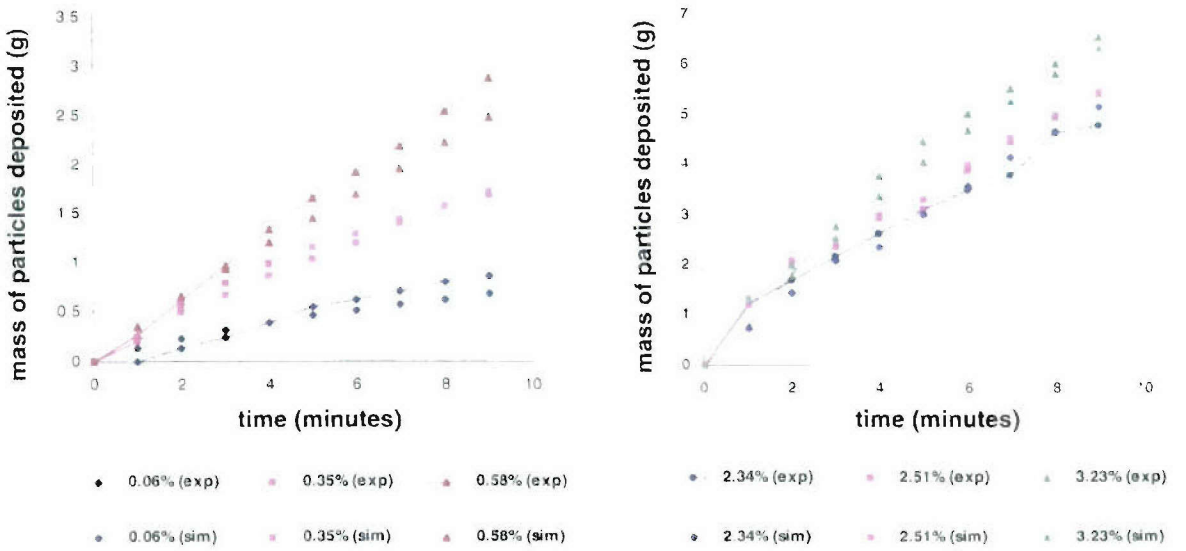

Figure 12 total mass of particles deposited as a function of time for various incoming concentration profiles, modeling (dashed) and experimental (solid lines) results

Task 4A: Process Developments: Evaluation of Membrane-Based Composite Processing

Background

The addition of a nanoporous membrane in the VARTM setup improves the quality of the final part. Thickness gradient and existence of dry spots are eliminated. Preliminary experiments have shown that the behavior of the membrane and its successful role vary with the resin used. Therefore, a fundamental understanding of the membrane is required. More specifically, we are interested in investigating and modeling the transport of resin through the membrane. Such a model will help us tailor a membrane for a specific application.

Review of the Work

This research follows the organization presented on the flow chart below:

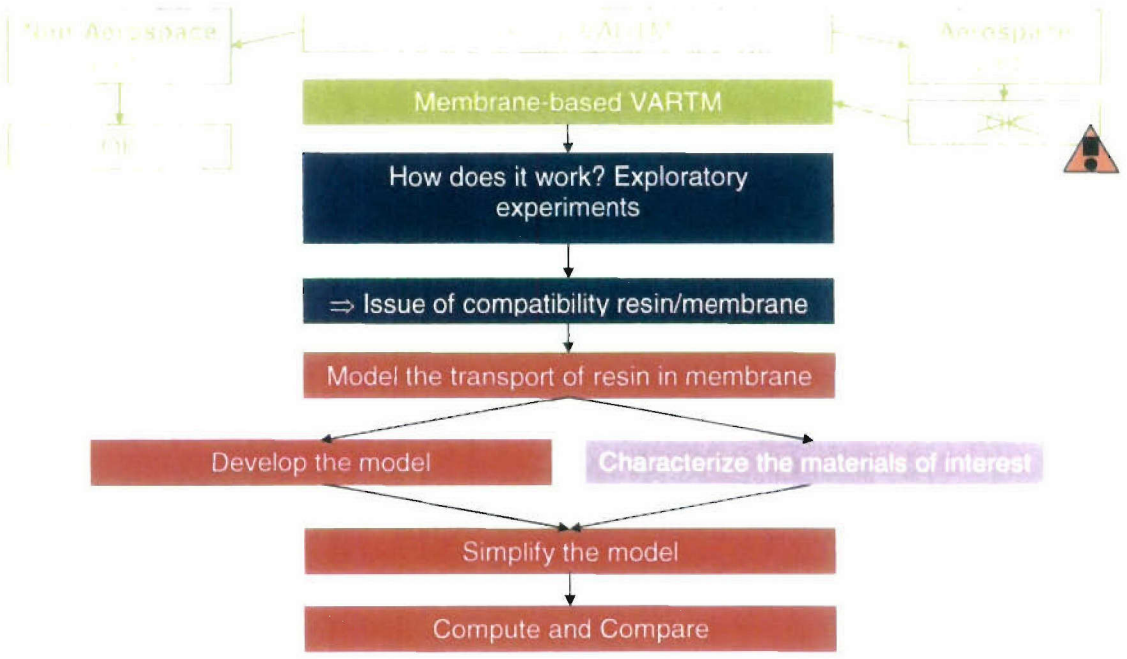

Figure 13 Flowchart of membrane-based VARTM work.

A previous report had detailed the exploratory experiments, which highlighted the issue of compatibility membrane/resin. The optical characterization of the membrane was also presented. This report is dedicated to the introductory model of resin transport through the membrane. Complementary characterization of the nanoporous medium is provided as well.

Wetting Characteristics of the System Membrane/Resin

To evaluate the wetting characteristics of the system membrane/resin, the contact angle between the two was measured. The setup (Figure 14) has the capability to provide not only

the static angle, obtained when the drop has stabilized onto the substrate, but also the dynamic contact angle, which is a measure of the contact angle as a function of time. In fact, a high-speed camera is used to capture the drop and, later, the evolution of the resin drop as enters in contact with the membrane. In the present case, since the resin possesses an intrinsic dynamic behavior (it cures with time and therefore its viscosity, wetting properties evolve with time), it is more accurate to deal with the dynamic contact angle. However, as a first approximation, the static contact angle has been measured.

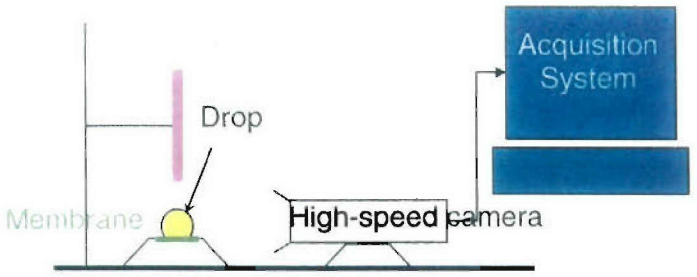

Figure 14 Contact angle setup.

Four fluids were tested.

1. The two resins which were used previously to make the VARTM parts for the so-called "exploratory experiments: Epoxy SC15 part A (resin part) and Vinyl-ester 411-350 + Styrene (ratio 1:6)
2. Vinyl-ester 411-350 alone
3. Styrene alone

These results (Figure 15) showed that the presence of styrene in the vinyl-ester dramatically lowers its contact angle. This can explain why the vinyl-ester+styrene system wetted the membrane and not the epoxy SC15 in the exploratory experiments.

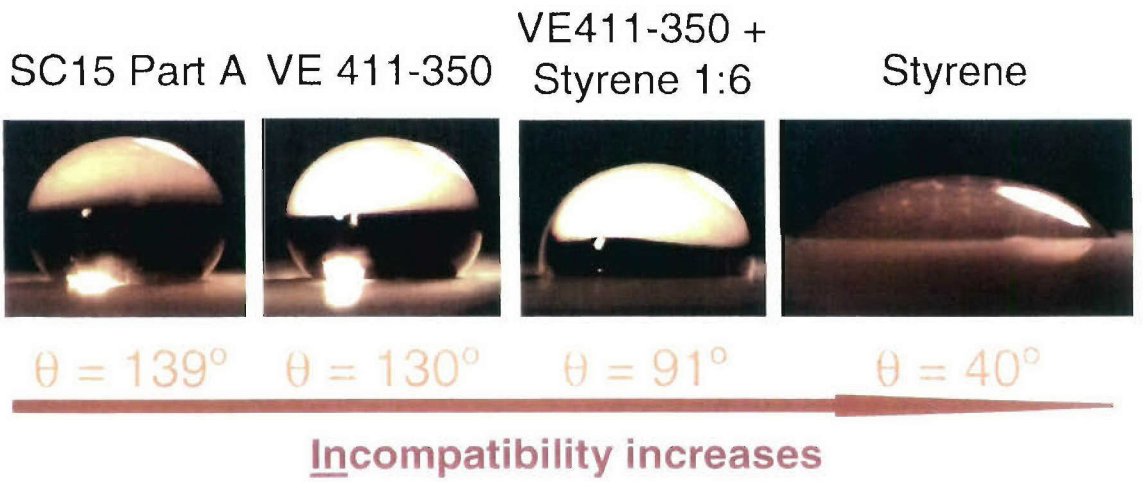

Figure 15 Results from the contact angle measurements.

Model

Ultimately, this project aims at designing membranes appropriate for all types of resin systems. In order to achieve this goal, it is necessary to make sure that the membrane will remain impermeable to the resin before it gels. In fact, once the resin hardens, there is no chance for the polymer to go through the membrane anymore. Therefore, it is key to know how long it will take for any resin system to go through the membrane. The model aims at predicting this time. The basis for this model is an introductory model, based on flow through porous media and capillary effects. Moreover, membrane and resin properties have been considered at their simplest, since there are no dynamic effects taken into account yet. Also, the geometry of the pores is simplified, as shown on Figure 16.

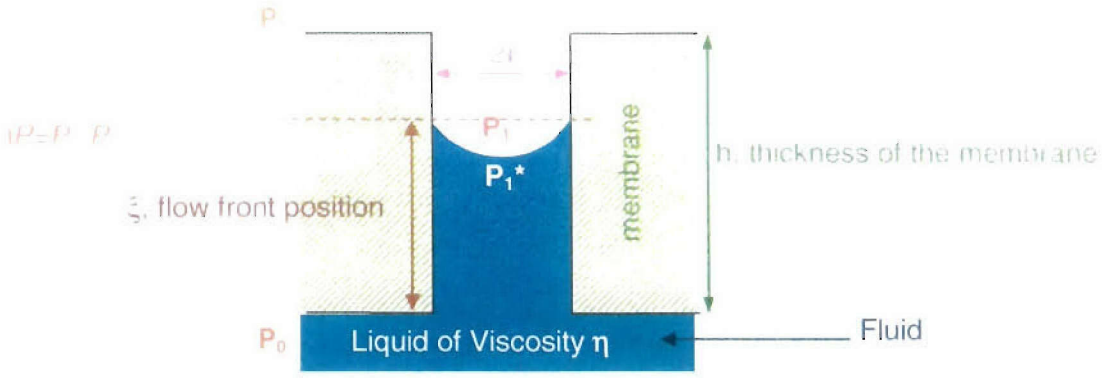

Figure 16 Schematic of a pore in the membrane.

There are three types of forces, which intervene in the wetting process. There is the vacuum applied on the membrane during the VARTM process and the maximum value it can reach is 105 Pa. Next is the capillary effect, which can either lead to a spontaneous motion of the fluid or prevent the liquid from wetting the surface without any external help. The last force to be taken into account is the gravity.

The model obtained is the following:

$$t = \frac{h^2}{\frac{2}{5}\frac{\varepsilon^3}{\eta S^{*2}}\left[\Delta P + \frac{2\gamma\cos\theta}{r} - P_g\right]} \qquad (2)$$

where h is the thickness of the membrane (m)
ε is the porosity of the membrane (%)
η is the viscosity of the liquid/resin (Pa.s)
S* is the specific surface area; in the case of a cylindrical capillary: m-1
ΔP is the pressure corresponding to the driving force (Pa)
γ is the liquid/resin surface tension (N/m)
θ is the contact angle between the membrane and the resin of interest
r is the pore radius (m)
P_g is the gravity pressure, which can be neglected

Thus

$$t = \frac{2}{5}\frac{\varepsilon^2}{\eta S}\frac{h^2}{\Delta P + \frac{2\gamma\cos\theta}{r}} \qquad (3)$$

It was found that the styrene alone can spontaneously wet the membrane and that the vinyl-ester resin system is also able to wet but only with the help of the vacuum applied during the VARTM infusion. These results are in good agreement with the experiments. However, the epoxy resin system cannot theoretically wet the membrane, even with the vacuum provided during a VARTM infusion. Since it does not correspond exactly to what was observed during the experiments, it is more likely that additional phenomena to the capillary effects play a non-negligible role. A possibility is that the contact of the epoxy with the membrane changes its wetting characteristics. In the future, the model will need to be improved to take into account the evolution of the wetting properties (surface tension, contact angle) with time and to give a more adequate description of the phenomena, which occur at very small times Additional characterization of the membrane is also required to better describe the microstructure.

Task 4B: Process Developments: Resin Bleeding During VARTM Infusion

The resin bleeding process which occurs after the complete resin infusion has significant influence on the final dimensional tolerance and fiber volume fraction of the composite parts. This study investigates the bleeding process using a finite volume method (FVM). The resin pressure and preform thickness distribution after full infusion are required as input data for the resin bleeding analysis. The contribution of material properties of the fibrous preform to the resin bleeding behavior is examined by adopting a characteristic time. The important material properties include the spring-back behavior of the preform allowing thickness differences in the part due to the pressure gradient during infusion. It is found that the preform with stiffer compaction property requires more time to reach a complete resin bleeding state, i.e., uniform thickness field throughout the preform.

Figure 17 presents schematically the pressure distribution after complete saturation of the preform. In contrast to typical RTM, the flexible vacuum bag allows thickness variation along the preform. The resin bleeding process is started when the resin injection line is closed. Because the vacuum pressure is still applied at the vent, the resin fluid is drawn out of the preform and the preform thickness and pressure gradient are reduced with time. Eventually, if the resin does not reach gelation state and enough time is elapsed, uniform preform thickness can be obtained.

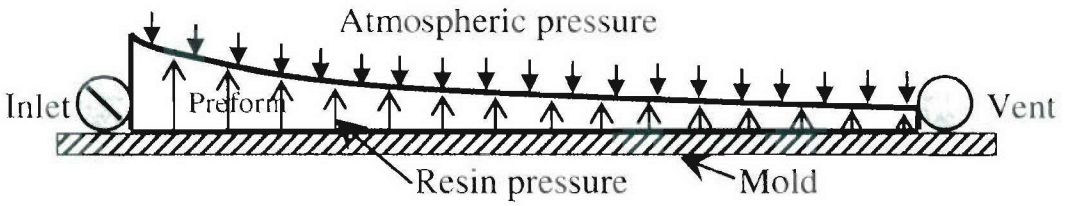

Figure 17 Schematic description of the pressure and thickness distribution after full infusion.

For the resin bleeding analysis, it is assumed that the system is compressible in the thickness, and incompressible in the in-plane directions. A one-dimensional non-rigid control volume as shown in Figure 18 is employed in the calculation. At both sides of the control volume, the flow rates are calculated and the overall volume decrease is computed with respect to time.

Figure 19 shows the change in resin pressure (Figure 19a) and preform thickness (Figure 19b) for the preform U812 (Vetrotex U812) during the resin bleeding process with a characteristic time $t_0 = \frac{\mu L^2}{k\Delta P}$ of 435s. P_0 denotes the inlet pressure and h_0 the preform thickness at the vent. After infusion and prior to closing of the injection line, the pressure at the injection port is 1 atm and reduces to 0 atm at the vent. The pressure gradient results in resin flow and a reduction in thickness and pressure at each preform location over time.

The simulation tool can be used to quantify the effect of VIP variations such as vacuum debulking or the changes in pressure in the vacuum or injection bucket on dimensional tolerances. In addition, sufficient gelation time to allow for enough resin bleeding reducing significantly the thickness gradient during VIP processing can be computed. The approach

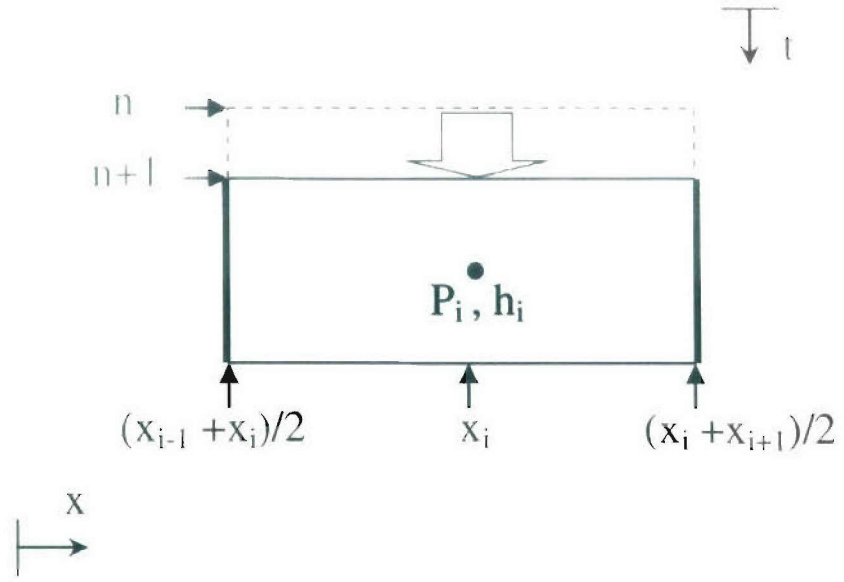

Figure 18 i-th non-rigid control volume employed for resin bleeding analysis.

allows insight in the important materials properties governing dimensional tolerances and can lead to improved part performance.

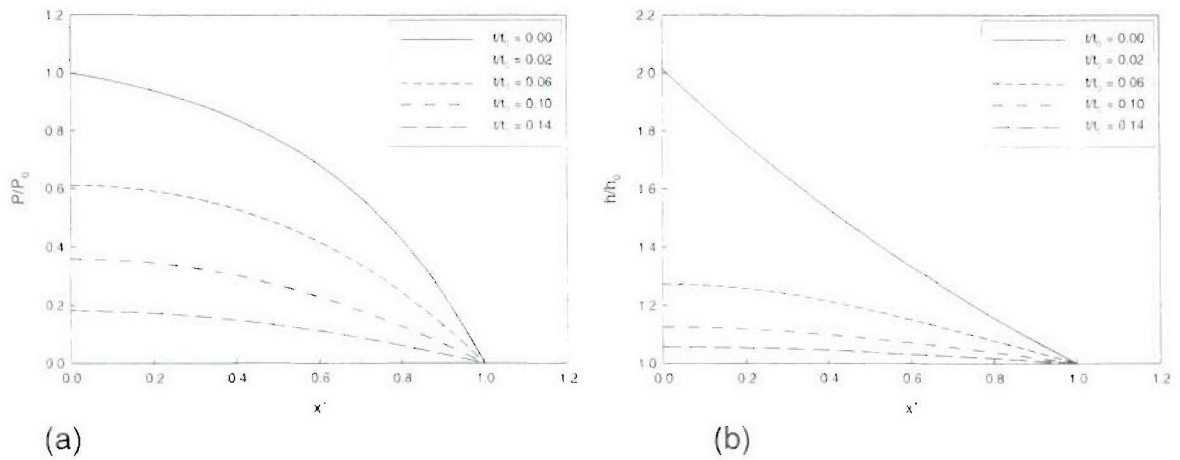

Figure 19 Change in (a) resin pressure and (b) thickness fields for preform U812 with respect to dimensionless time.

Task 5: Optimization of Distribution Media Lay-Up

In order to optimize the lay-up of distribution media, first one must be able to characterize distribution media and fabric permeability values during the Vacuum Assisted Resin Transfer Molding (VARTM) process. In VARTM, the available pressure for resin injection is limited to 1 atmosphere. Therefore, layers of high-permeability fabrics, called the Distribution Media (DM), are included in the lay-up to enhance the resin flow. During injection, resin flows initially in-plane saturating the DM, and subsequently through the thickness impregnating the bulk preform. Therefore, the DM permeability governs the planar resin flow pattern and lead length, which is defined as the difference between the flow position in the DM and in the bottom layer of preform adjacent to the tool surface. The lead length plays a critical role in successful infusion and is the key to optimization of the distribution media network. Thus, in this task, we investigated the DM permeability as a function of the preform layout. A new permeability estimation method, called Permeability Estimation Algorithm (PEA) that uses a numerical process model instead of analytical relationships, was developed. The flow chart that explains the methodology is presented in Figure 20. Subsequently, it was used to find preform permeability in the thickness direction and the in-plane distribution media permeability from one experiment using the flow front data from a uniform flow experiment. The accuracy of PEA was validated in the virtual environment. PEA was also used for permeability measurements in 1D flow experiments and its results were verified. Table 1 shows results measured in three experiments using PEA and 1D flow experiments for verification.

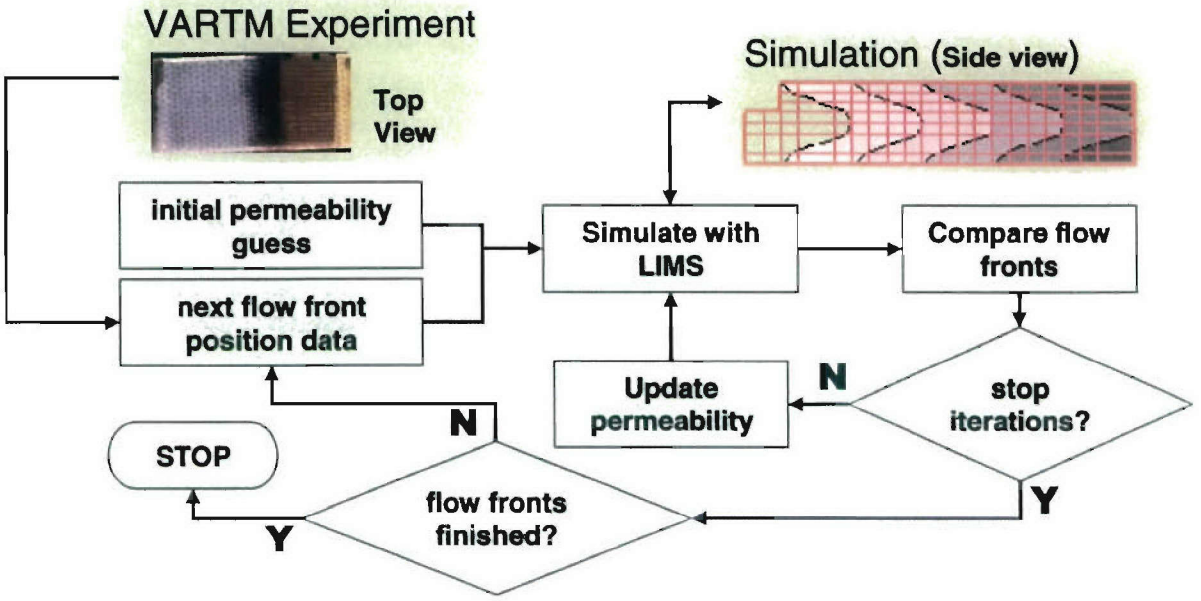

Figure 20 Flowchart of Permeability Estimation Algorithm (PEA).

PEA, unlike existing experimental permeability measurement methods, allows one to calculate permeability of different materials in the same lay-up. As PEA uses a numerical simulation and an iterative solver, it can be adjusted to accommodate various configurations and the flow does not have to be 1D. For example, it can be used to measure the permeability of a preform despite the presence of racetracking; or it can be used to find the principal permeability values of a preform using flow data from a radial injection. The results presented show that PEA converges on accurate permeability estimates asymptotically, hence it is stable.

Table 1 Comparison of permeability estimates in 1D flow by 1D flow Analysis and PEA.

Exp ID	K_{DM} - 1D analysis (m^2)	K_{DM} - PEA (m^2)	Standard Deviation
1	$4.998 \cdot 10^{-10}$	$4.995 \cdot 10^{-10}$	$2.12 \cdot 10^{-12}$
	$1.338 \cdot 10^{-9}$	$1.408 \cdot 10^{-9}$	$4.95 \cdot 10^{-11}$
	$4.467 \cdot 10^{-9}$	$4.446 \cdot 10^{-9}$	$1.48 \cdot 10^{-10}$

In this task, PEA has been successfully applied to permeability measurements in VARTM, revealing the fact that DM permeability depends on the VARTM lay-up; hence it should be measured in situ. Many VARTM systems of interest are increasingly using a combination of materials (e.g., graphite and glass) which makes permeability assessment difficult from a purely closed-form analytical approach. The PEA provides a means by which such hybridized systems can be accommodated and a reasonable estimate of the permeability field obtained.

Note that numerical methods inherently include some level of error. PEA finds the permeability estimates that reproduce the actual flow data. If the same finite element model is used for both PEA and other tasks (optimal design, process control etc), then numerical error introduced into the solution will be reduced. Note that error in measurement of pressures will cause an error in the estimations as shown in Figure 21. The details of this task have been accepted for publication in the following manuscript:

> Ali Gokce, Mourad Chohra, Suresh G. Advani and Shawn M. Walsh, "Permeability Estimation Algorithm to Simultaneously Characterize Distribution Media and Fabric Permeability Values in Vacuum Assisted Resin Transfer Molding Process," *Composites Science and Technology*, Vol 65/14, pp 2129-2139.

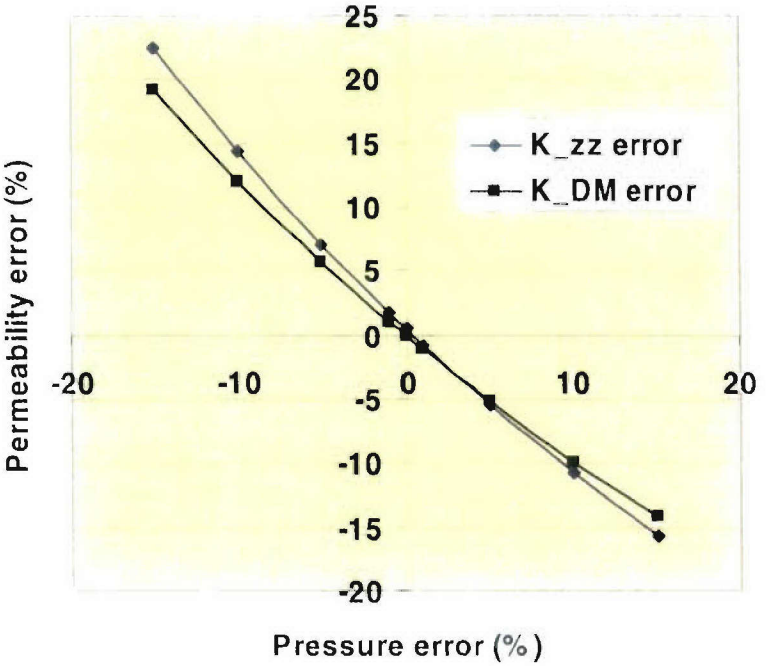

Figure 21 Permeability estimation errors as a function of input errors in injection pressure.

Task 6: Smart Actuator Development for VARTM

A Robot-Controlled External Vacuum Chamber for Resin Flow Modification During VARTM

To complement existing resin flow control strategies currently under development for VARTM and to provide the ability to react to unexpected changes in resin behavior during injection, a new technique for resin flow manipulation has been investigated to combat void formation. A unique, reactive technique for resin flow modification involving a rigid external vacuum chamber placed over the vacuum bag has been developed and tested. Using the chamber, a robotic system has been prototyped that identifies dry regions forming during injection, deploys the vacuum chamber over the mold, and actuates the chamber in order to modify and correct the resin flow within the mold.

External Vacuum Chamber Development

The purpose behind the external chamber is to provide some sort of rigid structure to shunt the atmospheric force acting on part of the perform and lift the vacuum bag, allowing the preform under the chamber region to spring back to a more relaxed state. The result is a gap between the bag and mold fibers that provides low resin flow resistance. Figure 22a is a schematic of the rigid vacuum chamber when activated over the vacuum bag. Preliminary testing with both round and rectangular chambers revealed the rigid chamber significantly affects the resin flow in the mold. The round chamber accepts inflow from multiple directions, which allows it to be very versatile; the rectangle chamber has a long action length, so its effect on the flow is more pronounced than that of the round chamber. The rectangle would be used in the most severe cases to rectify major flow front anomalies. The chamber's effects are controllable and depend solely on the application time of the chamber: as the chamber is applied for longer time periods, the effect on the flow becomes more pronounced and a greater volume of resin is stored in the gap[1]. When the chamber is released, the stored resin is forced into the preform for almost instantaneous impregnation. The excess resin also flows forward, enhancing the effect of the chamber even after its release.

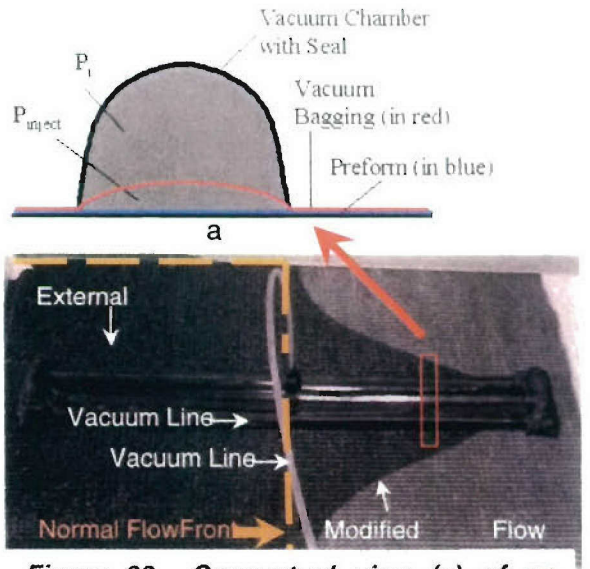

Figure 22 Conceptual view (a) of an external vacuum chamber and effects of the external chamber on resin flow (b).

Tests were performed to measure the effects the external chamber could have on part geometry or quality. Experiments were run with the long chamber in place on the part, and once the part was cured, it was cut laterally to obtain a cross-section of composite at the chamber location, which allowed part thickness measurements to be made at critical locations across the width of the part. The average thickness variation at the center of the chamber is 0.93%, and the thickness variation at the contact point of the chamber is -2.57%; this difference was not statistically significant. The change in fiber volume fraction was also statistically insignificant by using the method of Analysis of Variants, with a 95% confidence level.

Robotic System Development and Testing

To assess the potential for the external chamber to be used a resin flow control (and correction) tool, a robot system was developed to identify resin flow problems, and deploy the external chamber. The four main subsystems of the robot system illustrated in Figure 23 are the robotic arm for moving the chamber in the three degrees of freedom; the REx chamber vacuum technology itself for void reduction; machine vision for resin flow detection; and void characterization software, to determine the size and location of the void and to determine the location where the REx chamber will be placed. The semi-automated system is built around the standard VARTM setup; a schematic of the system level concept for the semi-automated flow control system is found below in Figure 24, with the major subsystems labeled.

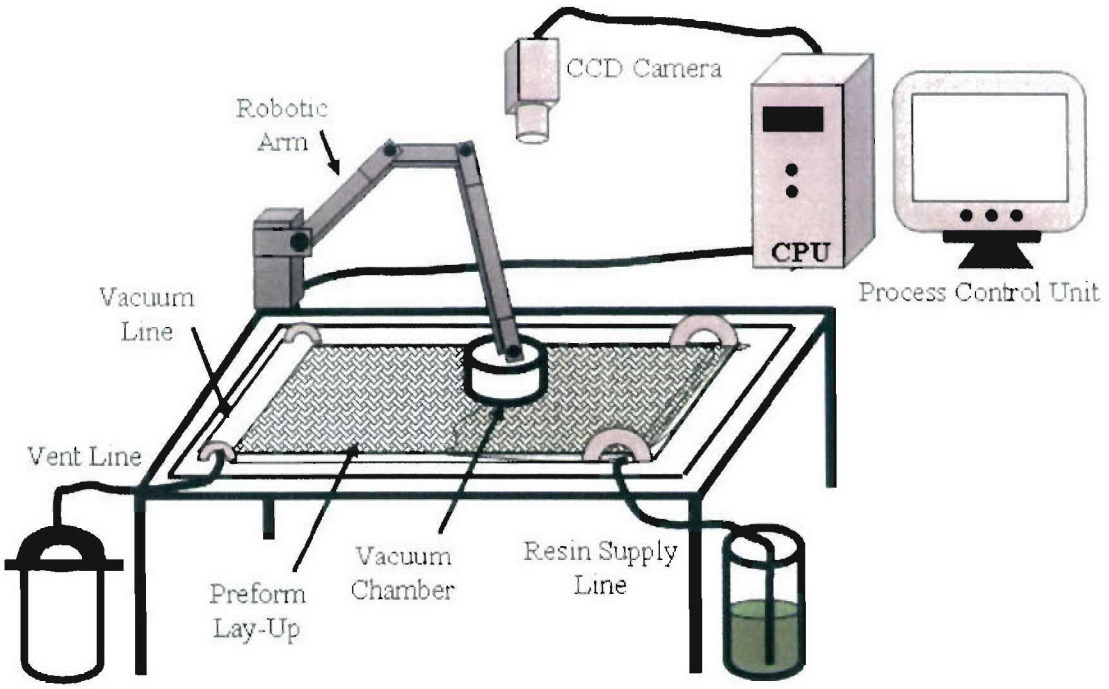

***Figure 23** Conceptual view of a VARTM injection system equipped with a robot that can position and actuate the external vacuum chamber.*

Figure 24 Main system components required for a flow modification system that utilizes an external vacuum chamber.

The core of the entire system is the process control unit, or process computer. Camera images are sent to the computer for analysis. The computer analyzes the images and based on the void characterization algorithm, the computer sends motion control commands to the robot arm. The computer also sends the activation and deactivation commands to the REx chamber itself which is attached to the robotic arm. In this way the major subsystems are integrated with each other to achieve maximum efficiency. The process computer uses LabVIEW® to interface with all components of the subsystems.

Figure 25 shows the prototype system equipped with a round chamber. Preliminary testing revealed the round chamber had limited effect on resin flow modification. Subsequent testing with a rectangular chamber (aspect ratio = 15) confirmed that a non-circular geometry significantly affected resin flow. Due to the long action length of the rectangular chamber, part of the chamber can be placed on the low-flow-resistance section of the preform and the resin can flow more readily into the chamber, while the rest of the chamber can be located on the void, where its action is most significant. Figure 25 shows the rectangular chamber being applied to the part to reduce the void.

Figure 25 shows the flow fronts for the control experiment and the robotically modified part at the same time. The dark patch (circled) in the modified part is excess resin pooled under the vacuum bag. Note that the flow front has been significantly modified by the implementation of the chamber. Also, note that the average flow front distance for the robotically modified part is more advanced than that of the control experiment. Upon completion of the infusion, the void is entirely eliminated with the use of the chamber. The excess resin under the vacuum bag acts as another resin source in addition to the injection line, which benefits the low permeability

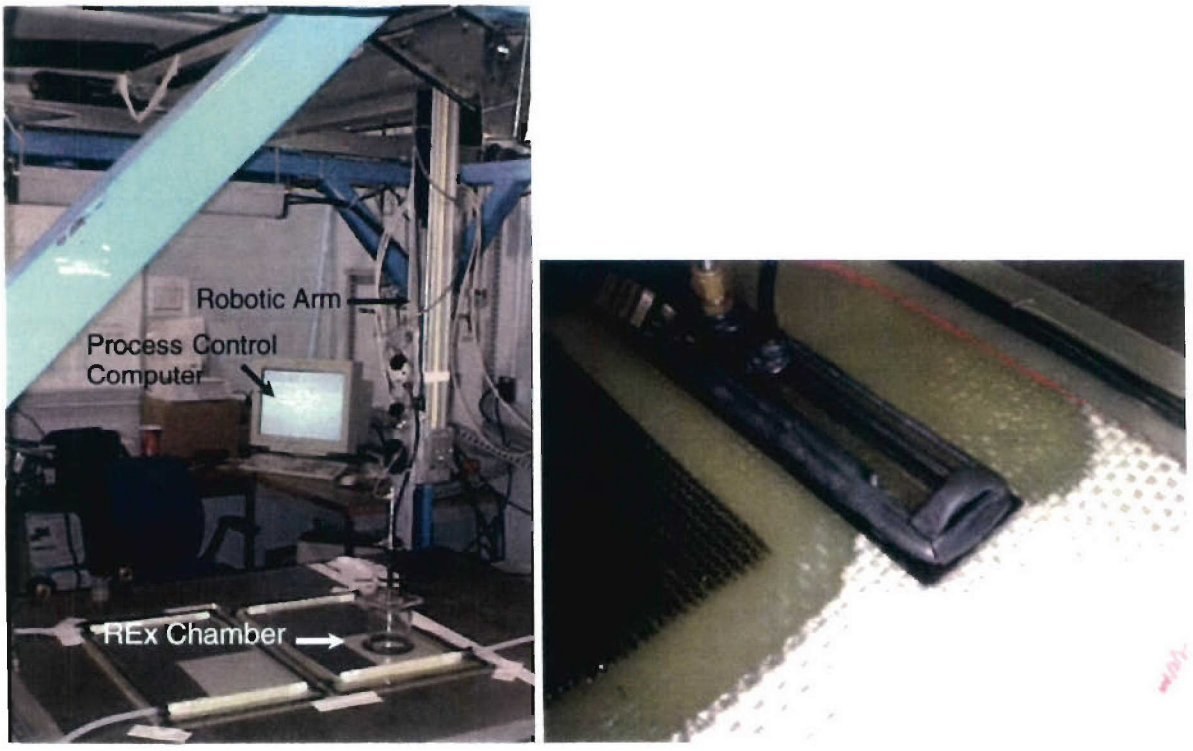

Figure 25 Prototype robotic system with a round REx chamber, and a closeup of the rectangular vacuum chamber during an experiment.

region because resin is available locally, without having to travel through a high-resistance zone from the injection line. By the time the injection is complete, the excess resin has been absorbed and there are no lasting effects on part surface finish. In addition to the total elimination of the void, the entire injection time is reduced by 15%-20%, which validates another metric that indicates the value and effectiveness of this method – reduced injection time is favorable.

Key Findings

The REx chamber method is a viable, efficient, and cost-effective way to reduce voids in the VARTM process. The REx technology itself is highly capable of altering the flow of resin during a VARTM injection. The proven ability of the semi-automated robotic version of the chamber technology to reduce (and even to eliminate) voids and reduce injection time means higher manufacturing productivity due to a higher success rate and a reduced cycle time, as compared to unmodified VARTM. In addition, the method reduces wasted resin caused by non-uniform flow fronts reaching the vacuum line at the different times, and reduces finished part waste caused by macro-void formation. In essence, the method pays for itself many times over by insuring successful injections. The method is also very simple; it relies on easily understandable vacuum principles already necessary for comprehension of how VARTM works, rather than on complicated rules for the proper ultrasound frequency needed for resin excitation, for example.

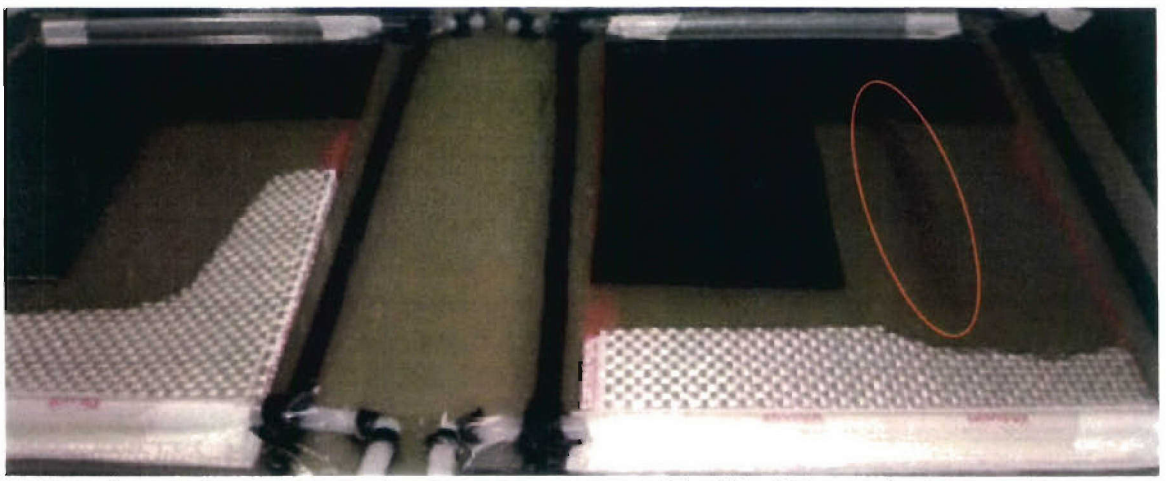

Experimental Control (no robot)

Modified Flow using External Chamber and Robotic Deployment

Figure 26 Flow Front Comparison Between Control (left) and Robotic Modification of flow (right). Note the large dry area on in the control injection, and the pool of resin (circled in red) that is present immediately after the REx chamber is removed.

Additional, this technique is usable, since nothing is permanently bonded into the finished product, which reduces costs compared to other flow modification methods in which some part of the method relies on disposable elements for success. Since nothing is bonded into the part, its mechanical properties must perforce be maintained; nothing about the composition of the finished product is altered.

Three potential implementations for the chamber exist: a fully manual version, a semi-automated version, and a fully-automated version. Each implementation has its own benefits and drawbacks in terms of cost, complication, accuracy, and consistency. The majority of the cost of the non-manual systems is indeed in the automation realm, and does not lie with the REx vacuum technology itself. Since the material for chamber construction is relatively cheap, custom shapes can be easily made to accommodate different injection geometries. Note also that this method is designed to overcome flow anomalies caused by slight variations in preform permeability over a large area, rather than anomalies caused by permeabilities that are orders of magnitude different, though experiments have proven that the chamber is capable of handling this type of situation as well.

Development of a Closed Loop Control Strategy for VARTM using a New, Segmented Resin Injection Line

Two active flow control strategies were designed and validated during this phase of the project. The first was a simple closed loop algorithm that used point sensors to feedback the resin flow position during injection. The second was a closed-loop adaptive routine that was realized by integrating LIMS into the controller program, thus providing the ability to simulate filling characteristics in real time. The controller was developed in Labview 7.1 and used the dynamic link library (.dll) version of LIMS to perform simulations during injection.

Closed-Loop Flow Control using Point Sensor Feedback (Strategy A)

Flow control strategy A is a closed-loop control method with point-sensor feedback; the basic control architecture is illustrated in Figure 27. The entire mold cavity is divided into m by n regions where m is the number of rows of sensors along the length of the mold and n is the number of injection line segments. For example, if the number of injection line segments used is 3 and the number of rows of sensors along the length of the mold is 6 then the entire mold region is divided into 6 by 3 regions resulting in 18 total sensors. Each sensor can be thought of as an indicator used to determine when a region has been filled with resin. Every segment of the injection line is assigned a group of sensors. For a simple rectangular mold like the ones considered in this study, the complete column of sensors in front of a particular segment are assigned to that segment. The command line feature of LIMS is used to incorporate the virtual sensors at the corresponding nodes in the mesh. The corresponding control logic developed for this strategy is presented in a flow chart in Figure 28. Initially all the injection segments are set as gates. The fill-factors of the sensors in the first row are then scanned using a script file in LIMS. LIMS assigns a fill-factor value of 1 to a node if it is filled with resin and 0 if it is dry. If all regions have a fill-factor of 1 for a given row of sensors, then the injection line segments are kept turned on and the next row of sensors is scanned and evaluated in a similar manner. Otherwise, the injection segments whose corresponding sensors in the row scanned have a fill-factor value of 1 are turned off and the resin infusion continues only from the other segments until the if-condition is true for the row. With this approach, the segmented injection line is used to correct the actual flow pattern by supply resin only to the region where the flow is lagging (i.e. where the fill-factor is still 0). Each row is continually scanned to identify regions with a "0" fill factor until the mold is completely filled. The injection segments are turned off when all the sensors have a fill-factor value of 1. The logic required to adopt this control strategy in LIMS is written in a L-basic script file which is interpreted using the command line input in LIMS.

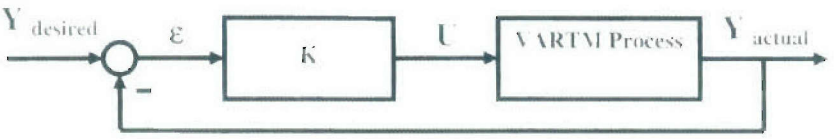

Figure 27 Controller structure for Control Strategy A.

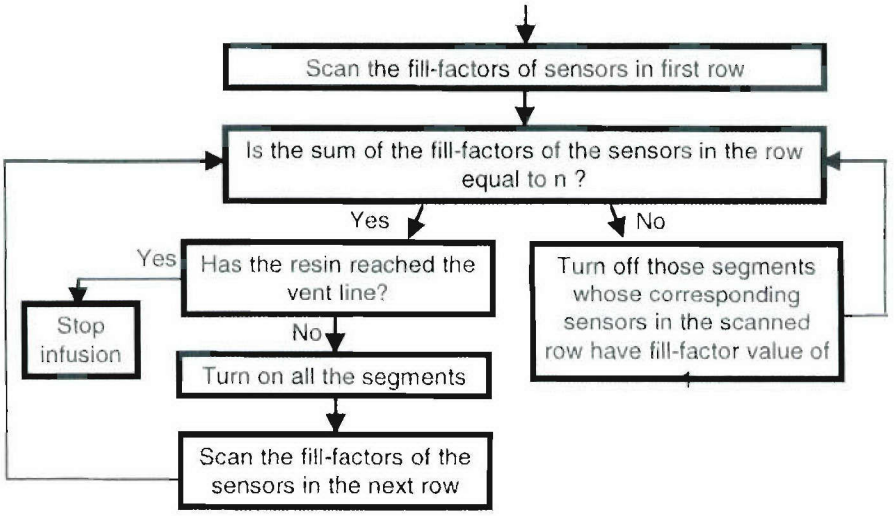

Figure 28 Controller logic for flow control using point sensors (Strategy A).

Model-Based Real-time Adaptive Flow Control (Strategy B)

Flow control strategy B uses a real-time adaptive control algorithm to modify resin flow. As illustrated in Figure 29, actual flow front position $Y_{actual}(t)$ is measured and fed back to a LIMS simulation model to determine the best injection line configuration U within the control time (dt) so as to progress the flow front to $Y_{desired}(t+dt)$. The implementation of this strategy essentially consists of two main parts. The first is the development of the process architecture and its components. The second is the development and implementation of the control algorithm in software. The essential components of the process architecture to implement control strategy B are the LIMS simulation software, script files to simulate the flow in LIMS, desired flow front shapes $Y_{desired}(t+dt)$ at various instants of time and distance along the length of the mold and various injection line configuration sets Ut+dt (the sets contained in Ut+dt are all the possible combinations of operation of the injection line segments in terms of "on" or "off" at the next time step). A virtual environment is used to simulate the flow and provide the optimum injection line configuration at different instants of time as the mold fills. This architecture of the adaptive closed-loop process controller is used to implement the control logic of strategy B presented in the flow chart in Figure 30. The finite element mesh of the mold with the preform and resin parameters, L-basic script files to simulate the flow in LIMS, injection segment data sets and the desired flow patterns at various instants of time are used to predict the flow for different injection line configurations in the time interval dt as well as the flow front position Y(t + dt)) for every possible injection line configuration. The predicted flow positions are then compared with $Y_{desired}(t + dt)$. The time (t+dt) is the time at which at least one of the virtual sensors in the next row along the length of the mold is filled with resin. The injection line configuration which

provides the smallest error between the desire and predicted flow fronts at time (t+dt) is selected as the optimal injection line configuration U. The injection line segments are then actuated and this procedure is repeated until the flow reaches the vent line. On the other hand, if the error is in the tolerable band at any time step the same injection line configuration is maintained.

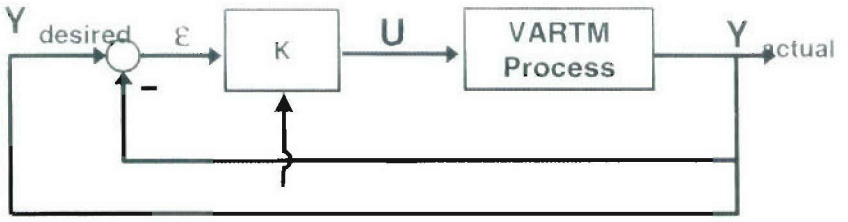

Figure 29 Controller structure for Control Strategy B.

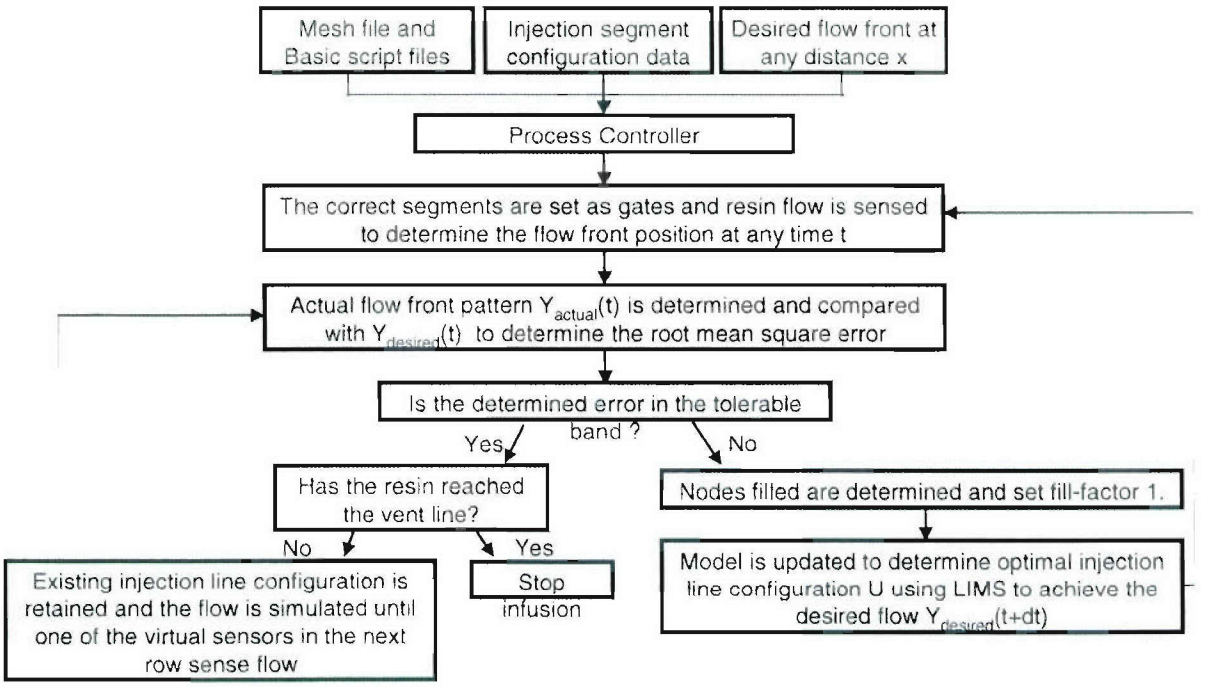

Figure 30 Controller logic for the real time adaptive control algorithm (Strategy B)..

VARTM Experimental Setup and Validation

To evaluate the performance of the segmented injection line and controller, a lab-scale mold was created. The conventional injection line was replaced with the segmented injection line. Based on the previous analysis of the resin flow for the lay-up pattern being studied, the number of segments in the injection line used for all the experiments was three. A schematic of the experimental set-up is shown in Figure 31. The regions of higher permeability within a preform lay-up were created by with additional layers of distribution media over those regions.

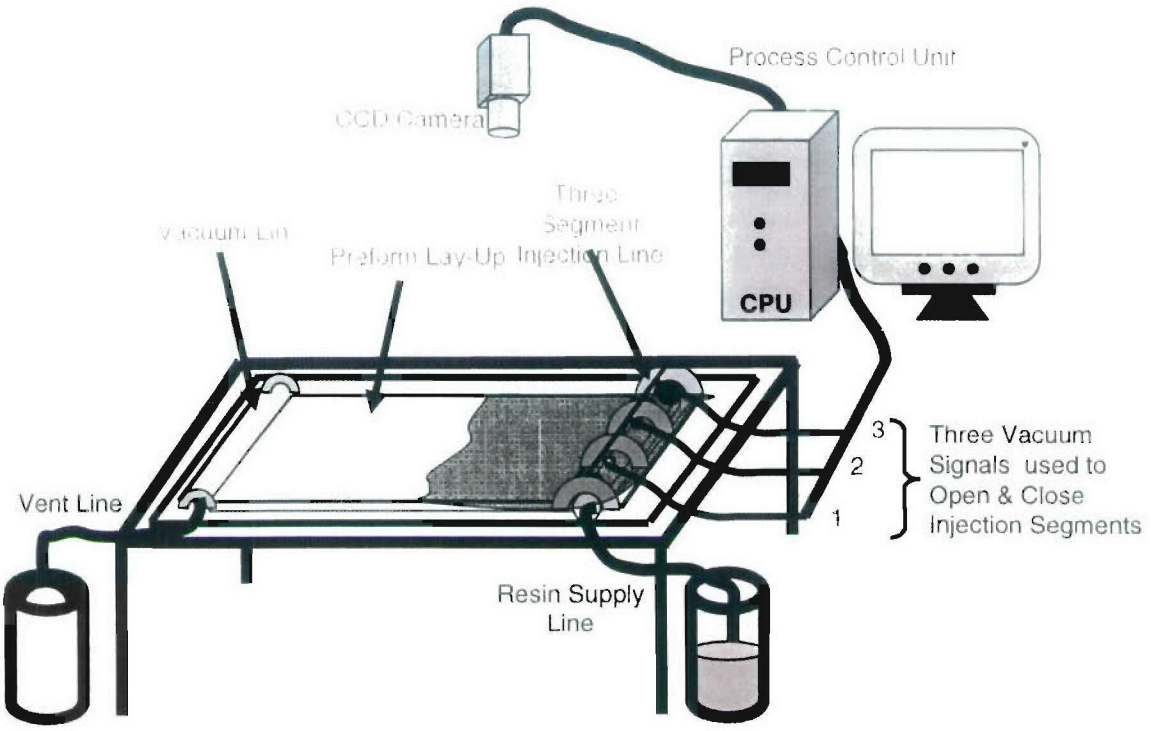

Figure 31 Experimental setup used to evaluate the segmented injection line.

The sources of vacuum to operate each injection line segments of the injection line were computer controlled through the opening and closing independent pneumatic solenoid valves. The control of vacuum chamber pressure for each segment was actually achieve with two valves; one was used to apply and hold vacuum (to open the segment) and the other to release vacuum and open the chamber to atmospheric pressure (to close the segment). A CCD video camera located above the mold was used along with a National Instruments IMAQ frame grabber card to measure the resin flow during the mold filling process. The mold region was grabbed at one second intervals and image analysis software was written to create a grid of virtual sensors from the mold image where each sensor corresponded to a particular region in the mold cavity. A 24 by 3 region grid was used for all experiments.

Evaluation of Control Strategy A

The opening and closing of the segments of the injection line were independently controlled with the algorithm presented in Figure 28 using virtual sensors created from the CCD camera image. Labview was used to implement the control algorithm and collect/compare image (virtual sensor) data, then actuate the appropriate injection line segment. The open loop characteristics along with the performance of strategy A are shown in Figure 32a and b, respectively. The measured void size was significantly reduced and indicates that this relatively simple algorithm in conjunction with the three-segment injection can significantly improve part quality where variations in permeability exist. Note that all experiments were terminated when resin first reached the vacuum line, even though the mold would eventually fill in some cases. As a result, strategy A was not able to completely eliminate the void.

Evaluation of Control Strategy B

The control algorithm logic illustrated in Figure 30 was implemented in Labview and utilized the LIMS dynamic library link for real-time estimates of the resin flow front. Prior to running

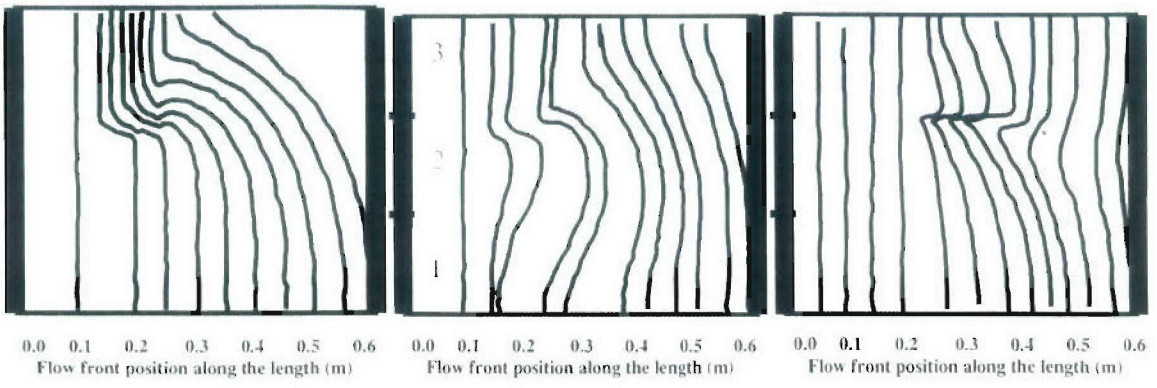

Figure 32 Measured resin flow boundaries at different stages of filling. (a) open loop response, (b) control strategy A, (c) control strategy B.

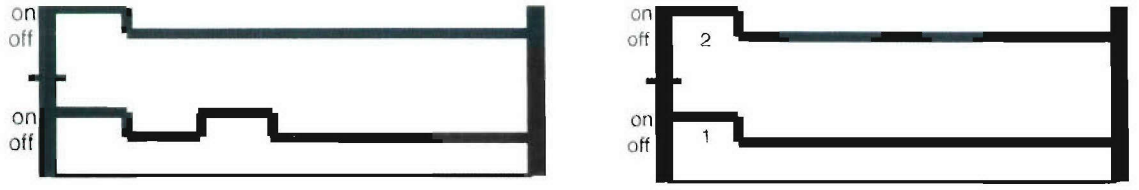

Figure 33 Control actions taken for (a) control strategy A and (b) control strategy B.

experiments, the effect of model size on processing time was examined. Tests were conducted with an Intel Pentium III, 1 GHz processor running Labview 7.1. Initial trials revealed that the number of nodes did have a significant effect on run time. Experimental results obtain with strategy B are shown in Figure 32c, and do indicate improved performance over control strategy A. in terms of void reduction. In fact, the void was eliminated for this mold configuration. Comparison of the controller actions for A and B (Figure 33) reveals a subtle but important difference between the two algorithms in which segment 1 was actuated for a short time under A but not B. The additional injection from segment 1 under A resulted in the flow front reaching the vacuum line before the mold was filled, thus creating a void. These results suggest that the benefits of the adaptive, model-based control may have performance advantages over the more simplistic sensor-based control algorithm.

Summary of Key Findings

A virtual experimentation environment with the integration of LIMS into Labview was successfully developed. Various active flow control strategies for VARTM using the segmented injection line were evaluated. These strategies were implemented in the virtual design environment and the performance of the segmented injection line was evaluated for different preform lay-up scenarios. The ability to control the resin flow in VARTM using the segmented injection line was demonstrated through both simulations and experiments. The integration of LIMS and Labview was successfully implemented as a part of the active flow control strategies. This new injection line technique has proven to be a very important strategy in achieving better flow control, especially where variations in permeability and complex mold shapes are present. Results indicate there is a significant decrease in the void area with the segmented injection line.

Optimal flow control was achieved by changing the lengths of the injection line segments and using suitable control action; both of which are mold dependent. In addition, an adaptive control algorithm that uses a finite element model to provide real-time updates of the injection line configuration was developed and implemented on a lab-scale mold. Experimental validation of two different control strategies demonstrates that real-time, model-based control is possible in VARTM and can be used to eliminate void formation during injection.

Task 9: Structural Monitoring of Composite Materials

Structural damage results in local stiffness changes, which affects the dynamic characteristics of the structure. A two-dimensional Gapped Smoothing Method can be used to determine the stiffness irregularity of a structure, and this information can be used to identify, locate, and quantify defects. The Gapped Smoothing Method requires Operational Curvature Shapes, which can be derived from experimental acceleration-based frequency response function (FRF) data. Traditionally these FRFs have been measured from a structure using a 'roving hammer' technique. One or more accelerometers are maintained at fixed reference positions, and the structure is excited with an instrumented hammer at each test point in a grid in turn. While setup of the experiment is reasonably quick, the actual data acquisition can be time consuming. Also, the procedure is not easily amenable to automation. This study investigates an alternative approach, which is to rely on the reciprocity principle. Rather than measuring the response at a few locations, and exciting a large number of points, the investigated method is to excite at a few points, and measure the response at a large number of points. The cost of hundreds of conventional accelerometers can be prohibitive, and therefore this project investigated using an array of low cost MEMS accelerometers. MEMS are also attractive in that they may be embedded into a composite structure during manufacture.

There are two different scenarios that can obtain the required array of FRFs. These are shown schematically in Figure 34. The first approach is to establish a few fixed reference accelerometers, and to excite the structure at each of the test points. This approach is comparable to the method used for experimental modal analysis with a roving impulse hammer, although analyzer configuration and test mesh density tend to be different for NDI. The second approach is to excite the structure at just a few locations, but this time the response is measured with an array of accelerometers, one per test point.

Fundamentally, the principle of reciprocity ensures the two different experimental approaches yield the same FRF data sets, since:

$$H_{jk}(\omega) = H_{kj}(\omega) \tag{4}$$

where j and k are the excitation and response coordinates respectively.

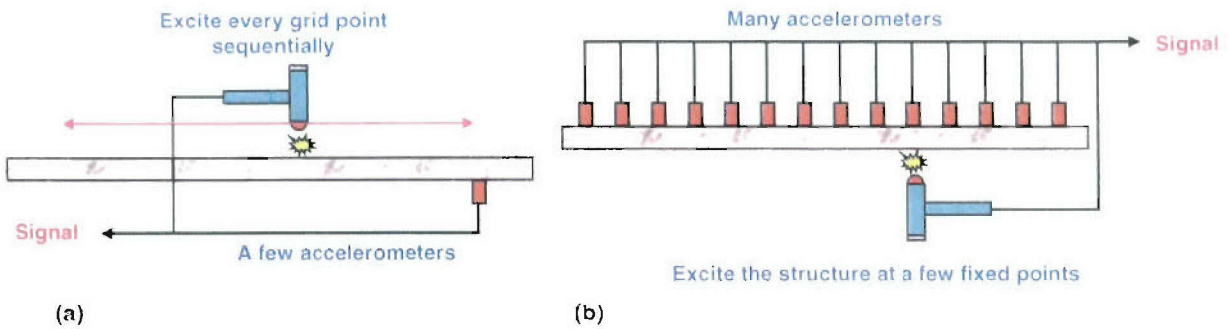

Figure 34 Experimental setup for two case scenarios.

- ***Case I: Multiple excitation with a few sensors***
- ***Case II: Single excitation with multiple sensors.***

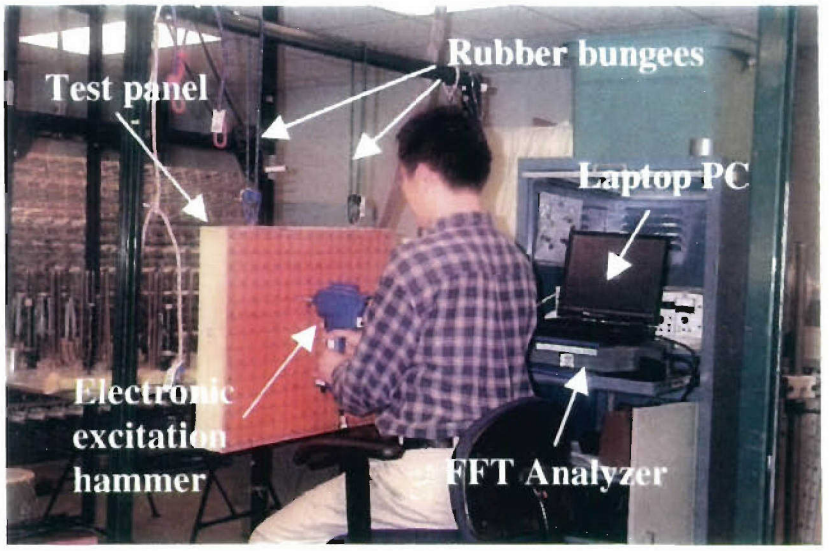

*Figure 35 **Vibration testing of a CIRTM sandwich panel..***

The use of this second approach, using an array of MEMS accelerometers, has not previously been investigated, and a comparison with the first approach is the major focus of this study. The laboratory-scale composite panel shown in Figure 35 measured 24.5 x 20.8 x 3.7 inches, and was manufactured for the US Navy as a potential fire test specimen. The panel had two 1.50 inch thick balsa cores separated by an E-glass/vinyl ester skin. The outer layer was E-glass/vinyl ester and formed the outer surface of the structure, while the seventh layer (E-glass/phenolic) formed the inside surface, and acted as a fire protection/retardant layer. The fifth layer was supplementary, and provided support the whole structure if the first layer was burnt away by fire.

The part was manufactured using the one-step Co-Infusion Resin Transfer Molding (CIRTM) process by Anholt Technologies, Inc. A circular Teflon film was inserted at the interface between the E-glass/vinyl ester layer and the balsa core during the manufacturing process to introduce a known defect. Also, a large delamination existed at the interface between the E-glass/vinyl ester layer and the balsa core. This was caused by a manufacturing defect where the layers were forced apart by the evaporation of entrapped water during elevated temperature curing. During vibration testing two rubber bungee cords held the composite panel to simulate an all-free boundary condition. A total of 224 (16×14) grid points were marked on the front surface of the panel with a 1.5 inch grid spacing in both horizontal and vertical directions. Two MEMS sensors (ADXL150) were placed at the upper right corner on both surfaces of the panel to obtain the dynamic responses of the panel.

Figure 36(a-b) show contour plots of the Structural Irregularity Indices obtained using the roving hammer test (Case I). Excitation was on the E-glass/vinyl ester side, and the responses were measured with sensors attached at the front and back surface of the composite panel, respectively. Both results identified the large elliptical delamination. Since the single accelerometer was located near the small circular delamination, the data should not be used to indicate that the damage was located. The reduction in the "sensor feature" in Figure 36(b) is directly attributable to the extra distance between the front-tested surface and the back-mounted accelerometer. The MEMS array results are shown in Figure 36(c-d). When excitation was on the front surface the "sensor feature" dominates the plot, although there is some indication that the elliptical delamination was located. Results from impacting on the back surface better

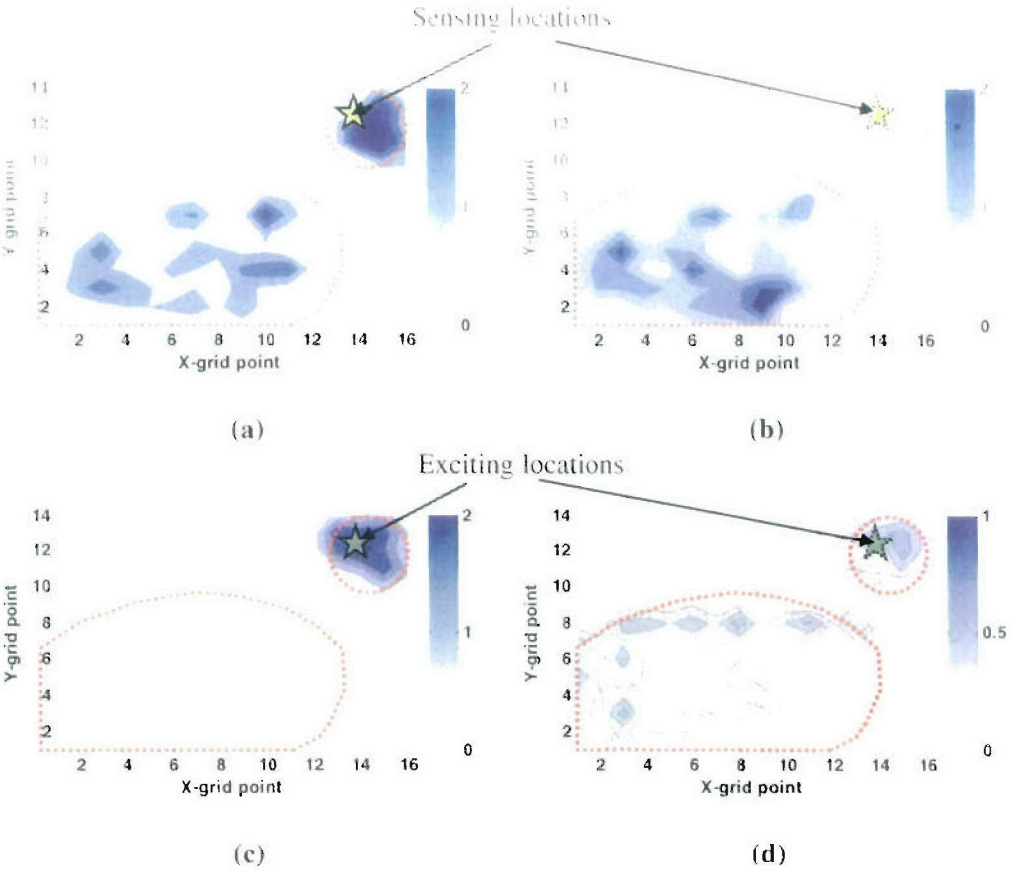

Figure 36 Structural Irregularity Index for the composite panel. (Dotted circles show delaminated areas; Star marks show exciting/sensing locations)

- ***Case I, Excite the front surface and sense at the front surface***
- ***Case I, Excite the front surface and sense at the back surface***
- ***Case II, Excite the front surface and sense at the front surface***
- ***Case II, Excite the back surface and sense at the front surface***

identify the elliptical delamination, but the results are not as clear as when using the roving hammer method. The mass loading caused by the MEMS sensors and their associated wiring changed location as the MEMS were moved one column at a time across the structure. It is speculated that this changing mass loading caused sufficient changes in the structural dynamics of the panel that the damage feature was reduced in magnitude when compared with the roving hammer method. This problem could be resolved by installing a complete array of MEMS and leaving it in situ throughout the test. There is also a possibility that the relative calibration of the MEMS may have caused some small variations in the measured data, similarly reducing the effectiveness of the procedure.

The second test article was an 8 x 4 x 4 foot composite structure, replicating the corner of a topside Director Room (Figure 37a), which is an electronic enclosure for the US Navy DDG-51 destroyer. The corner structure consisted of three composite sandwich panels with the same configuration as the previous panel. They were also fabricated with the CIRTM process. The corner structure was a prototype and it contained manufacturing defects (delaminations) caused by trapped water vapor that evolved during the elevated temperature cure. Figure 37 (b) shows the outside surface (E-glass/vinyl ester), where the delaminated areas can be observed as

lighter colored regions. The defects on the inner surface (E-glass/phenolic) cannot be identified visually because the phenolic resin was opaque, Figure 37(c). During testing the structure was stood upright, with the 8-foot side in the vertical direction. The bottom of the structure was isolated from the ground using rubber isolation pads. All surfaces of the structure were marked with a 6-inch-square test mesh for a total of 315 test points. For this structure both ICP (309A, PCB Piezo-electronics, Inc.) and MEMS (ADXL150) accelerometers were used in order to compare their performance.

(a)

(b)

(c)

Figure 37 Composite topside ship structure (fabricated by Anholt Technologies, Inc.). (a) CIRTM manufacturing process of the corner structure; (b) Inside of the corner structure; (c) Outside of the corner structure

Figure 38(a-f) show contour plots of the Structural Irregularity Indices obtained using the roving hammer test (Case I) and MEMS array (Case II). In these figures the dashed line identifies the visually-located delaminations. It is interesting to note that the damage is so severe that when the reference point was at point "A", the damage-related Structural Irregularity Indices have a larger magnitude than those caused by the operating curvature shapes transducer anomaly discussed earlier. When the reference is within the boundaries of the delamination, Point "B", the Structural Irregularity Indices increase in magnitude near the transducer, but the major delamination is still identified. One of the main aims of the work reported here was to verify that both the roving hammer and MEMS array test protocols were valid. Comparing Figure 38 (a, c,

e) and separately comparing Figure 38 (b, d, f) it can be seen that there is excellent agreement between the two roving hammer tests (one using high quality ICP accelerometers and the other using low cost MEMS accelerometers). When comparing the roving hammer (Case I) with the MEMS array (Case II), there are some differences in the lower-valued details. However, the overall shapes of the plots are similar, the main damage features are equally well identified, and the magnitudes of the Structural Irregularity Indices are comparable.

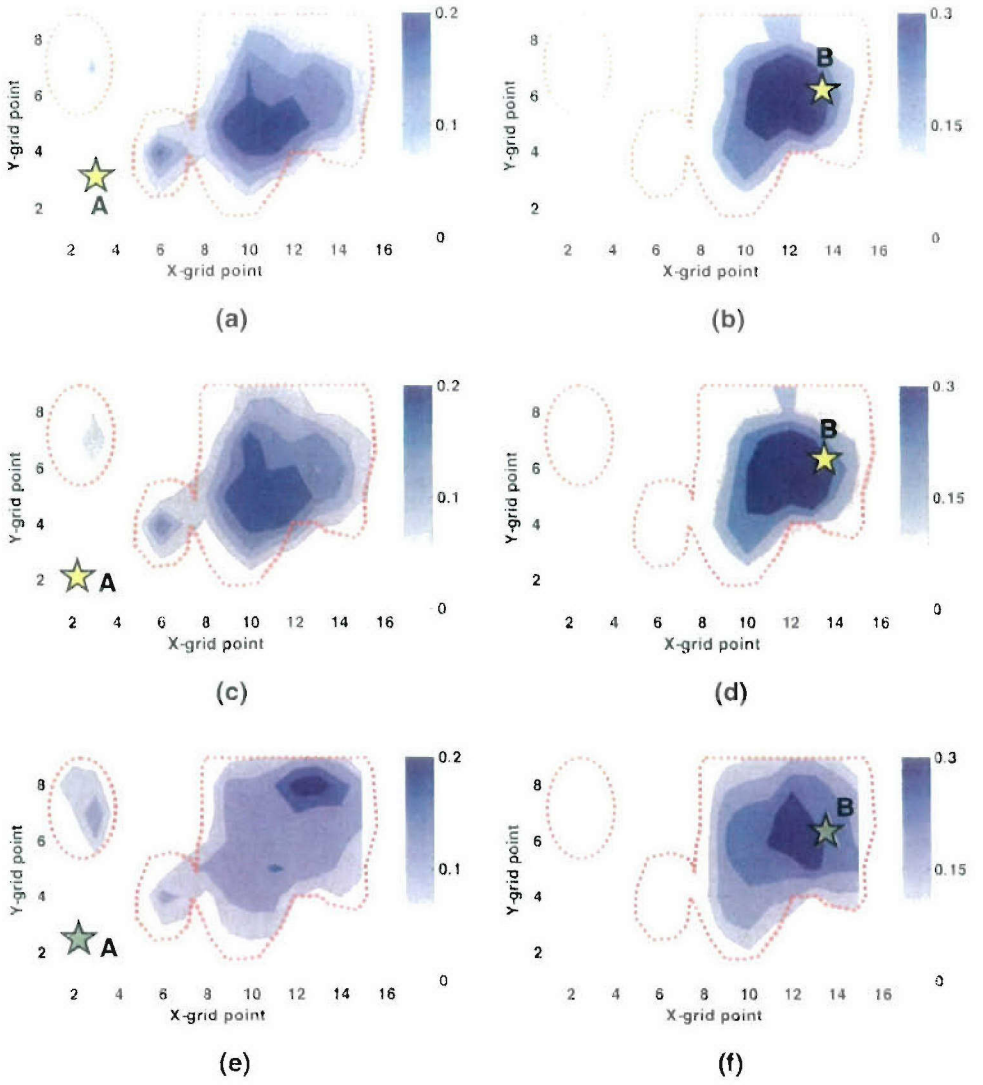

Figure 38 Structural Irregularity Index for the composite corner structure.
(Dotted areas show delaminated areas; Star marks show exciting/sensing locations)

- *Case I, Excite the front surface and sense at the location A with ICP*
- *Case I, Excite the front surface and sense at the location B with ICP*
- *Case I, Excite the front surface and sense at the location A with MEMS*
- *Case I, Excite the location B and sense at the front surface with MEMS*
- *Case II, Excite the location A and sense at the front surface with MEMS*
- *Case II, Excite the location B and sense at the front surface with MEMS.*

In all of the roving hammer cases the ICP and MEMS results were highly comparable, with only small differences. These results indicate that low-cost MEMS sensors have sufficient fidelity for use in vibration based NDI methods. The technique using a MEMS array of sensors is an enabling technology for full automation and remote diagnostics for the health monitoring of large-scale in-service structures. Future work includes developing natural excitation methods such as vehicle induced vibration for bridges, engine induced vibration for aircraft wings, and airflow induced vibration for helicopter turbine rotor blades.

Task 10: Intelligent Design of Prototype Molds for Injection and Control in RTM

(VA)RTM Workstation

Previously, a workstation was designed and built to facilitate research and prototype development for the RTM process. This workstation is able to quickly and easily manufacture various part geometries, as well as providing individual control to several inlet gates and vents distributed over the surface of the mold. Embedded sensors provide information about the flow progression without interfering with normal molding procedures. Finally, all components are tied together with a supervisory computer and software to provide automation and data logging during the experiments. Recent years have seen the increase in popularity of the VARTM process, and it was therefore desired to utilize the workstation for VARTM research as well.

Upon initial experiments, it was discovered that vacuum was quickly lost inside of the mold cavity. While leakage was initially suspected as the cause of the problem, further investigation discovered that the vent channels providing vacuum to the mold cavity were being blocked off due to the lower membrane separating the piston and molding plate. What was happening was that initially, a strong vacuum would be pulled in the mold. The vacuum in the channels was sucking the membrane up against the top plate, thus sealing the channels from the mold cavity.

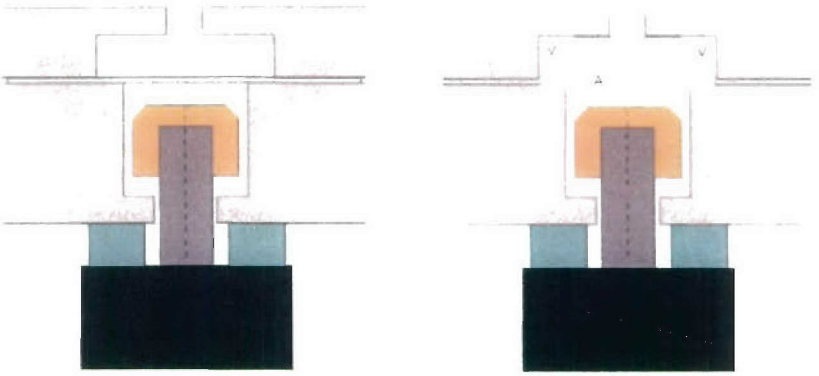

The solution was to draw vacuum under the lower plate, since it was the air coming through the pistons that is pushing the membrane up against the vacuum inside the channels.

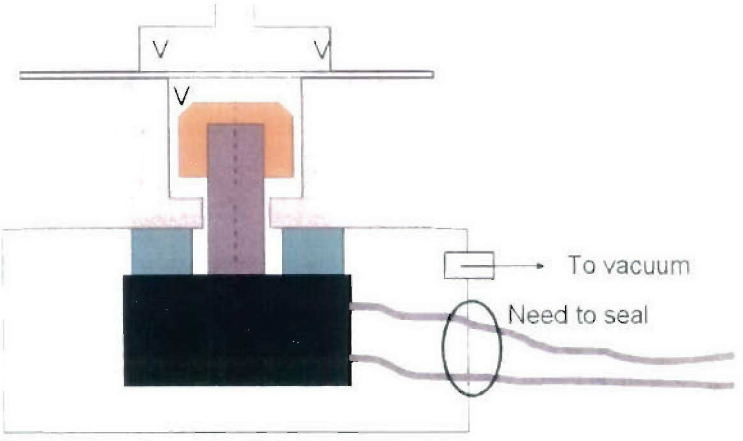

Therefore, a design was made to encase all of the pistons in a large chamber. Then, vacuum could be pulled inside the chamber, thus neutralizing the pressure level above and below the membrane. This would maintain the membrane in its proper place, and allow for vacuum to be maintained in the mold itself.

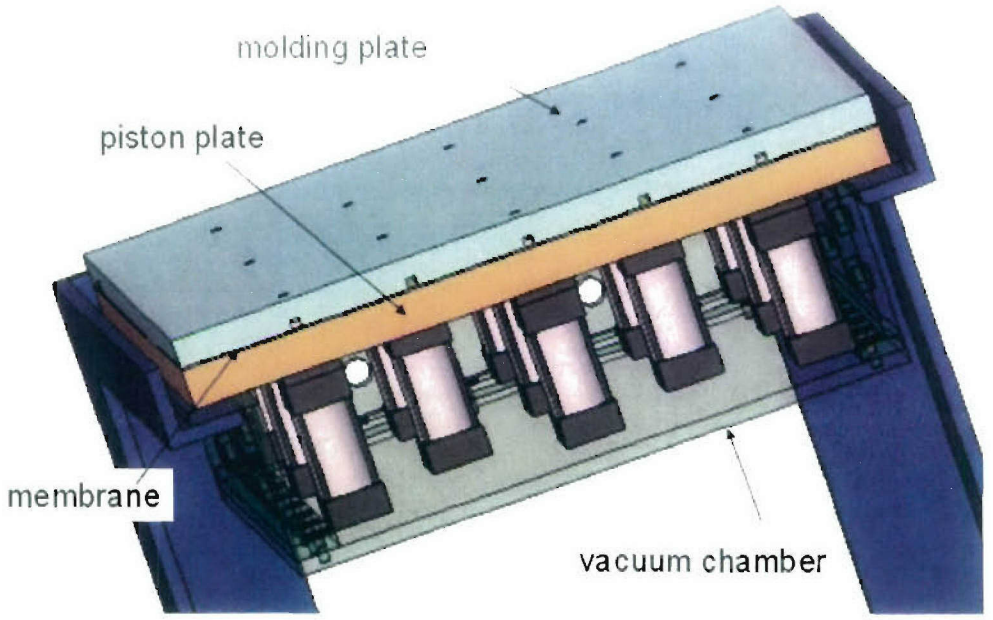

With this design, the vacuum chamber was designed and built from acrylic. It was installed into the workstation. Testing demonstrated that applying vacuum to the chamber did neutralize the pressure across the membrane, thus ensuring the membrane would stay down with vacuum applied in the channels.

Next, experiments were conducted to see how manufacturing using this apparatus compared to standard VARTM infusion. The major difference between using this apparatus and traditional manufacturing is that the gates and vents are located on the molding surface, as opposed to on the bag surface. Distribution media needs to have a direct connection to the main injection gate, so that the fluid can be easily distributed over the preform. Since the gates are on the mold surface, and the distribution media is typically placed on the bag surface, this is not immediately possible. The solution entails draping the distribution media over the end of the preform, and connecting it to a gate not covered by the preform itself. Therefore, the fluid will emerge from the gate, connect immediately to the distribution media, and flow through the distribution media, and finally through the preform itself. The only concern is to place some highly permeable material (such as additional layer of distribution media or breather cloth) between the distribution media and gate so that the vacuum bag does not collapse into the channels in the distribution media, and slow down the flow.

With all of these precautions, it was found that experimentation went very well. The bagging process was even easier than traditional VARTM, due to the absence of omega tubing that created the need for vacuum bag pleating. With the cleaner, easier bagging process, leaking is less likely, as the majority of bag leaks occur due to the pleating.

The photo below shows the setup, and demonstrates the draping of the distribution media past the fabric edge with breather cloth placed underneath to avoid collapse.

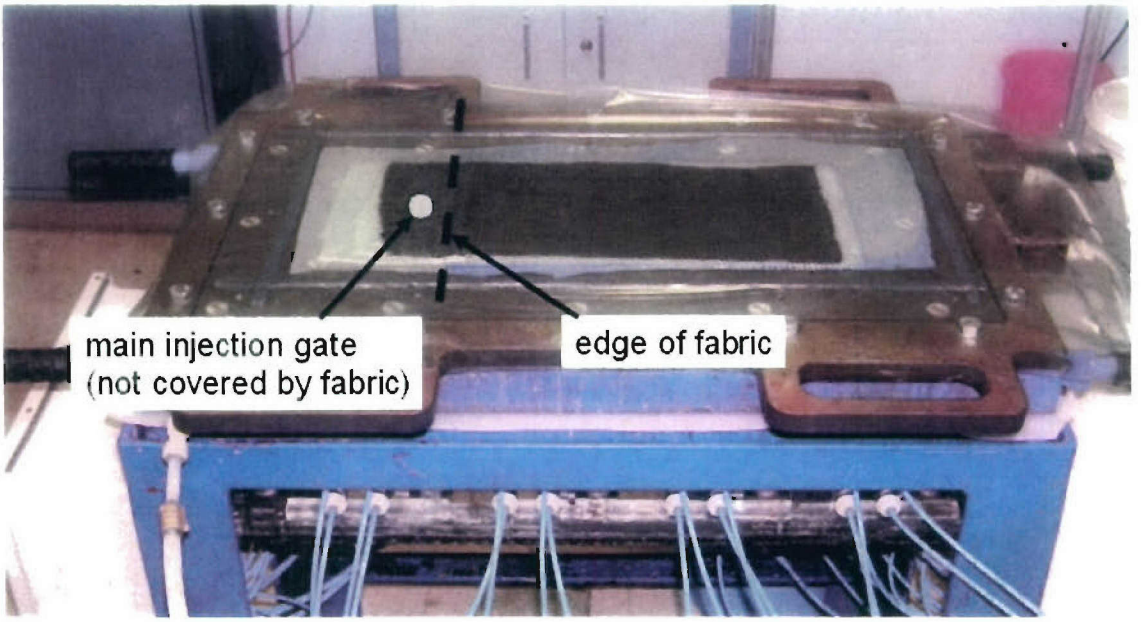

Task 11: Technology Transfer Test-Bed - Infusion of Tall Structures

The present study investigates the infusion behavior including gravitational effects for various tall structure infusion scenarios. A closed form analytical solution including gravitational effects and friction losses within injection tubes is developed to capture the process physics unique to tall structures. Flow front locations and resin fill times have been examined for a wide range of process values to evaluate processing limitations and optimum processing conditions. Experiments have been conducted to investigate the resin flow front and pressure distribution and to validate the analytical model for several different infusion scenarios. Sensors integrated in the tool provide real time data on the pressure distribution and flow front locations. Case studies include infusions of two fabrics of different permeabilities at various inclination angles and flow directions. The basic assumptions for the resin flow are that the fluid is Newtonian and incompressible, the flow is one-dimensional and laminar in the tube and preform, resin has constant density and temperature, the reinforcement is homogenous with constant porosity and permeability, and the tubing and perform have constant cross sections. Figure 39 shows a schematic diagram and the coordinate systems of the one-dimensional VARTM tall structure manufacturing process.

The resin arrival time changes due the gravitational forces applied to the resin. Combining continuity and momentum equations with Darcy's law leads to the following equation for the flow time:

$$t = \frac{\phi\mu}{\bar{K}\rho g \sin(\Theta)}\left\{ s + \left[\frac{8\bar{K}W_m H_m L_t}{\pi R^4} - \frac{P_r - P_v}{\rho g \sin(\Theta)} + \frac{L_v}{\sin(\Theta)} \right] \cdot \ln\left[1 + \frac{s\rho g \sin(\Theta)}{P_r - P_v - \rho g L_v} \right] \right\} \quad (5)$$

where P_r is the vacuum pressure of the resin bucket; μ is the viscosity and ρ is the density of resin, respectively; g is the gravitational constant, K is the permeability in the preform, and ϕ is

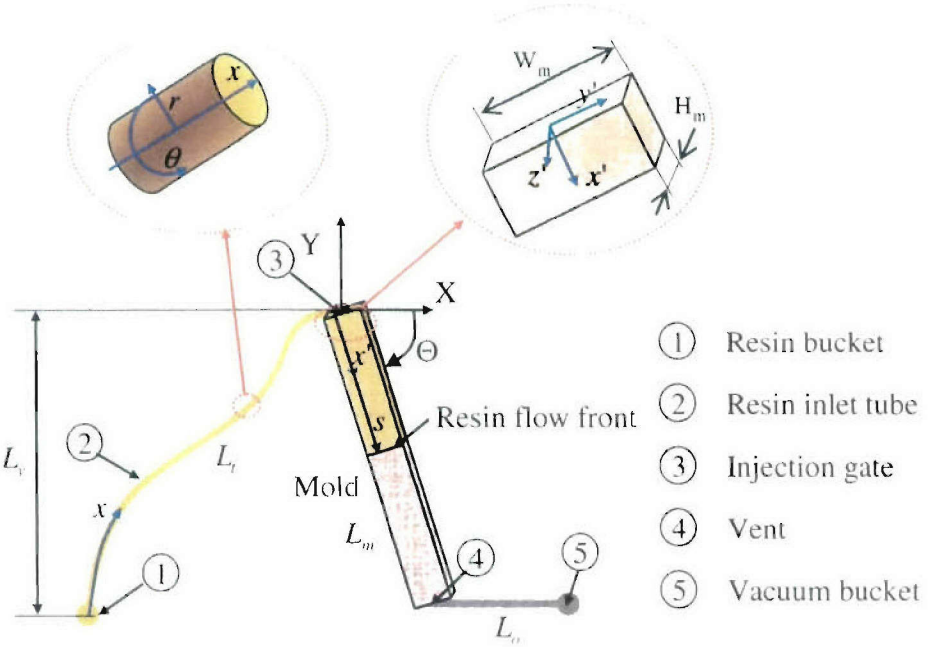

Figure 39 Schematic diagram and coordinate systems of the tall structure resin infusion system.

the porosity of the perform. Using the following dimensionless variables:

$$s^* = s/L,\ t^* = (P - P_0)t/\mu,\ k^* = K/L^2,\ g^* = \rho g L^2/(P - P_0),$$
$$a^* = W_c H_c / L^2,\ r^* = R/L,\ l_h^* = l_h/L,\ L_t^* = L_t/L \tag{6}$$

Equation (5) can be rewritten as the following non-dimensionalized equation:

$$t^* = \frac{\phi}{k^* g^* \sin(\Theta)}\left[\frac{s^*}{g^* \sin(\Theta)} + \frac{1}{(g^* \sin(\Theta))^2}\ln\left(1 + g^* \sin(\Theta)\, s^*\right)\right] + \frac{8\phi a^* l_h^* s^*}{\pi (r^*)^4 \left(1 - g^* L_t^* \sin(\Theta)\right)} \tag{7}$$

If the resin flows downward in the preform (i.e., $\Theta = 90^\circ$), and if the tube loss is negligible ($L_t = L_h = 0$), then Equation (7) becomes as follows:

$$t^* = \frac{\phi}{k^*}\left[\frac{s^*}{g^*} - \frac{1}{(g^*)^2}\cdot \ln(1 + g^* s^*)\right] \tag{8}$$

If the gravitational effect is negligible ($g^* = 0$) and the mold and tube are horizontally located (i.e., $L_t = \Theta = 0$) but the tube loss is included, Equation (7) becomes as follows:

$$t^* = \phi\left[\frac{(s^*)^2}{2k^*} + \frac{8a^* l_h^* s^*}{\pi (r^*)^4}\right] \tag{9}$$

If both the tube loss and gravitational effects are neglected, Equation (3) becomes:

$$t_0^* = \phi (s^*)^2/(2k^*) \tag{10}$$

where t_0^* is the reference dimensionless resin fill time. Equation (10) provides the flow time typically associated with the one-dimensional Darcy's law.

The relative resin fill time with the dimensionless gravitational term (g^*) as defined in Equation (2) is shown in Figure 40 (Assuming no friction and head losses in the injection tube, i.e.,

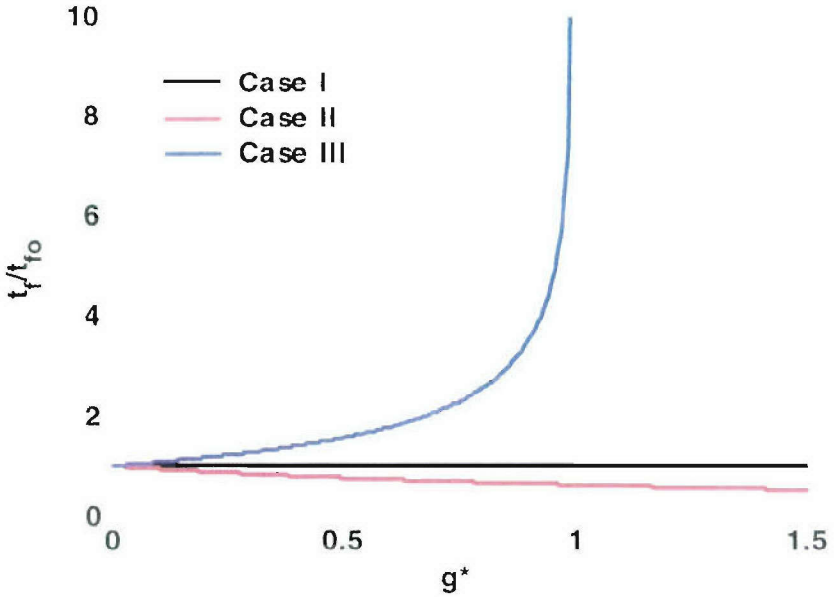

Figure 40 Relative resin fill time with dimensionless pressure (g^*).

$L_f = 0$). Relative resin fill time reduces as the dimensionless head increases for Cases I (horizontal infusion) and II (downward infusion). The graph also illustrates the significant height limitations of the upward infusion scenario (Case III upward infusion). Resin cannot fully impregnate the preform when the dimensionless head is over 1 for Case III. Therefore, there is a limitation in the length of the mold as a function of resin density and infusion pressure when resin is injected upward, while there is no limitation in the length of the mold when resin flows horizontally or downward in the VARTM process.

Figure 41(a) and (b) show comparison of the results between experiments and simulations with the analytic solutions using the two different preform materials. Dotted lines show experimental results and solid lines show those from the analytic solution. The resin fill time at the 4-meter mark was 7, 4.2, and 14 hours for the Airweave preform with predicted values of 7, 4.9, and 14 hours showing very good agreement between model prediction and experimental validation results. The shading cloth has higher permeability and thus exhibited faster flow times. The experimental values show 4-meter mark arrivals times at 20, 16, and 35 minutes for the shading cloth for Cases I, II, and III, respectively. The arrival times only differed slightly for Case III, which can be explained by local variations of the preform permeability and/or slight changes in the resin viscosities. However, overall the model was able to quantify accurately the increase/decrease of the fill time for the two different materials and in all process variations.

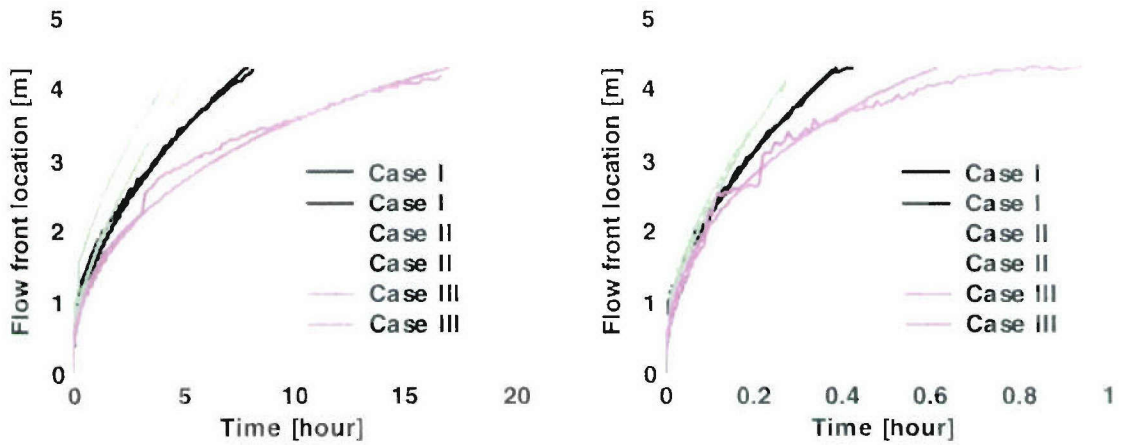

Figure 41 Validation of analytic solution with experimental results. (Dotted lines show experimental results and solid lines show those from the analytic solutions.).

Task 12: Conformal Antenna Array

In this study, the feasibility of manufacturing embedded antennas using VARTM process and the structural performance is investigated. The primary focus is on the integration of Copper radiating elements into structural skins and the associated issues of manufacturing and performance. Traditional antenna systems are integrated into structures by cutting out sections and replacing with 'conformal' patches. This approach requires additional local reinforcement to maintain structural performance. This study focuses on integrating antenna elements directly into structural composites during the manufacturing process and if feasible, can enable integrated manufacturing of antennas in structural composites.

The resulting component is a multifunctional material, which has to meet structural and dielectric requirements. Components that are embedded in the structure to impart dielectric properties may cause the structural properties of the part to suffer. Our goals in this stage are:

- To enhance the bonding between the Copper inserts and the composite structure, through the use of surface treatments.
- To characterize the effect of antenna components on the structural performance of the structure: Specimens with inserts of varying dimensions in them will be manufactured. The flexural, tensile and compression properties of these specimens will be measured and plotted as a function of the *insert area / part area* ratio.

While there has been extensive research on the adhesion between copper and glass fiber/epoxy composites, there has not been very little attention devoted to adhesion between copper and glass fiber/vinyl ester composites. Compared to cured epoxy, cured vinyl ester has comparable mechanical properties, higher water resistance and better dielectric properties. Thus, vinyl ester resin system is a good candidate material, especially, for telecommunication applications in marine industry. The goal of this work is to evaluate the adhesion between copper and glass fiber/vinyl ester composites and develop methodologies to improve it.

As-received copper foils were treated using different methods in order to control and improve the adhesion between Copper and E-glass fiber/vinyl ester composites. The peel strength behavior and failure modes for copper/glass fiber/vinyl ester systems with various surface treatments were investigated and compared to those for copper/glass fiber/Epon epoxy baseline system. The results indicate that the baseline copper/glass fiber/Epon epoxy system peel strengths were twice that of the untreated copper/glass fiber/vinyl ester system. Four surface treatments for copper were evaluated: co-cured Epon/vinyl ester, fully cured Epon, γ-MPS silane and epoxy film adhesive. Results showed that the average peel strengths were 61%, 101%, 96% and 105% of the baseline copper/glass fiber/vinyl ester system, respectively. Compared to the copper/glass fiber/Epon epoxy system, fully cured Epon, γ-MPS silane and epoxy film adhesive surface treatments had equivalent peel strengths, The peel strength results also show fluctuations that

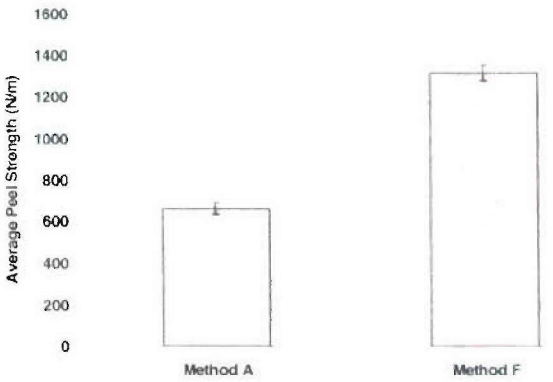

Figure 42. Adhesion performance of copper/glass fiber/vinyl ester (Method A) compared to that for copper/ glass fiber/epoxy (Method F).

were significant for samples with fully cured Epon (12%) and epoxy film adhesive (17%) treatments, compared to all other samples.

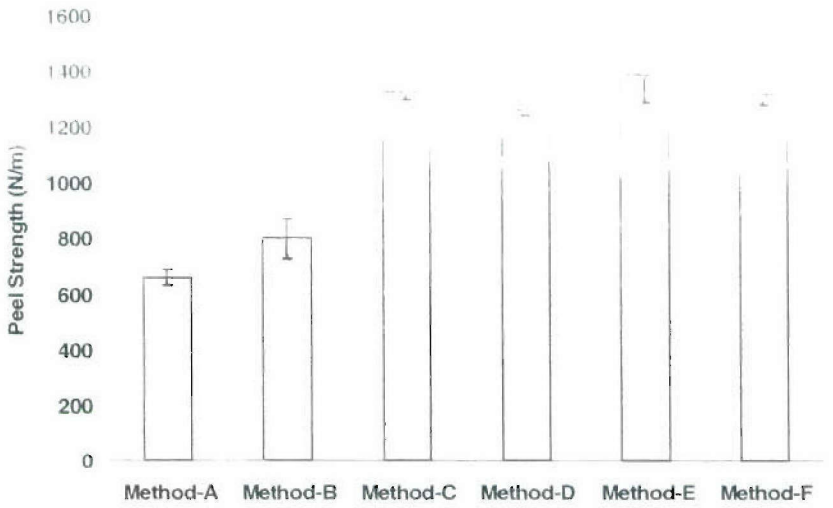

Figure 43. Average peel strength measured for copper specimens, with different surface treatments bonded to vinyl ester (A – untreated; F – bonded to epoxy).

In our approach the radiating elements are structurally incorporated with glass fiber/vinyl ester composite (which serves also as dielectric medium). We used the copper inserts as radiating elements. For conformal antennas, the location and geometry of radiating elements are restricted with application as well as the frequency range desired. They can be applied in different configurations such as grid copper and copper coated Kapton copper, or spiral configuration and small copper batches printed with a grid configuration on a dielectric substrate. Moreover, Epoxy/glass fiber substrates are usually used as dielectric medium, but in our work, the glass fiber/vinyl ester composites were selected as reinforced material and dielectric medium, which are good candidate materials for water immersion applications.

It has been shown that the adhesion between copper and vinyl ester is poor and therefore, the overall structural performance of the composite becomes an issue. So, the copper surface has to be mechanically and chemically compatible with composite constituents, otherwise, the copper inserts become non-reactive inclusions (i.e. defects) in the structure, causing the structural integrity to degraded. There is a shortage of data published on the structural integrity of glass fiber/vinyl-ester composites with embedded copper inserts. The present work can fill this gap by evaluating the structural properties for glass fiber-vinyl-ester composites with copper inserts taking into consideration parameters such as the copper size and the copper surface-substrate adhesion.
When the conformal antenna structure is placed in an application, it can be exposed to different loading modes depending on the construction of the antenna structure. Laminates are typically subject to flexure loads, while for a conformal antenna as a part of a sandwich structure, the compression and tension modes are significant. Thus, the present work focuses on structural properties under tension, compression, and flexural loading for glass fiber-vinyl-ester composites with copper inserts.

However, adhesion between copper and vinyl-ester is important, as poor adhesion will degrade structural properties. In our previous investigation, it has been shown that for copper-glass fiber/vinyl ester system, the application of a thin interlayer of Epon 828 epoxy to the copper surface will result in a copper-substrate adhesion increase of 100%. This method of copper surface treatment was also applied in this work to enhance the overall structural performance of the composites having copper inserts with different area ratios. The types of testes and copper inserts applied in this work are listed in Table 2.

Table 2. Structural Performance Test Matrix

Test	Copper Type	Insert Area Ratio (%)
4-Point Bending	Bare Copper	0, 2.8, 11.1 and 44.4
	ETP Copper with as-received treatment	44.4
	ETP copper treated with Epon 828 Epoxy	44.4
Tension	ETP Copper with as-received treatment	0. 3.6, 7.1, 14.3 and 28.6
	ETP copper treated with Epon 828 Epoxy	28.6
Tension/Compression	ETP Copper with as-received treatment	0, 0.9, 3.6, 14.3 and 57.16
	ETP copper treated with Epon 828 Epoxy	57.16

The mechanical properties of the manufactured composites containing various size inserts were investigated using four-point bending, tension and compression tests as a function of the insert size.

The mechanical response of the specimens tested in tension exhibited a shift from pure elastic behavior to bilinear behavior for large inserts. Furthermore, the ratio of elastic modulus to non-elastic (E_2/ E_1) and elastic strain have a decreasing trend as the copper area ratio increased, whereas the tensile strength and the Poisson`s ratio were not affected by the insert size. Compared to tension loading, the compressive and flexural loadings have stronger impact on the measured mechanical properties. The tensile compressive properties (strength and strain at failure) showed a remarkable decrease in their values as the insert size increased. The specimens tested in flexural loading did show a significant degradation in elastic stress/strain values and failure properties associated with compression mode as the size of the insert increased. These significant losses in the structural properties can be attributed to the poor adhesion between the copper surface and the composite. The poor copper/composite adhesion can also explain the failure modes observed by the specimens tested. The specimens tested under tension showed several failure modes such as delamination and fracture in the composite structure and copper inserts, where the larger scale delamination was observed by the specimens with larger copper inserts size. For the specimens tested under flexural loading, the observed failure modes, such as interfacial delamination, fiber/matrix fracture at edges of the insert and copper buckling became more intensive and pronounced for specimens with larger insert size. Similar failure modes were observed by the specimens tested in tensile compression.

A surface treatment of copper inserts with Epon 828 epoxy system resulted in a significant impact on the improvement of the copper-composite adhesion through which the structural

properties were significantly improved. Using this surface treatment, the losses in the compressive strength properties became negligible compared to baseline specimens and the flexural elastic stress/ strain (end of elastic region properties) associated with compression mode were improved 130% compared to specimens with "Bare" copper inserts. Besides the improvement in the compressive and flexural properties, the surface treatment also has an impact on the failure modes observed by the specimens tested. The surface treatment with Epon 828 minimized the interfacial delamination and the buckling failures in the specimens tested in compression and inhibited the copper buckling, interfacial delamination of the compression side of the specimens tested und flexural loading.

Task 14: Analysis of Dynamic Blast and Material Characterization Techniques

Quasi-static experimental techniques under uni-axial stress and uni-axial strain conditions are revisited to study the axial compression behavior of crushable cellular materials for blast applications. A new class of cellular core materials with composite webs and polymeric foams is identified as a potential material for blast application. Blast experiments on large sandwich panels have revealed that the supports are the most vulnerable places for damage. However, the damage behavior of structures under blast can be studied using static test methods. Limited modeling efforts have been undertaken to understand the effect of the mass properties on overall blast responses of structures. It has been found that cellular composite sandwich structures transfer momentum from the front face sheet to rear face sheet through the composite web. Composite web structures also change the global deformation behavior allowing local deformation of the face sheets between webs. Future studies are planned to investigate the effect of 3D composite-foam hybrid core structures for optimum energy absorption under blast loading.

Quasi-Static Axial Compression of Cellular Materials and Sandwich Composite.

The energy-absorbing behavior of cellular materials under blast loading can be investigated by quasi-static axial compression (Figure 44). Balsa core is widely used in marine structures. While the critical stress of closed cell aluminum foams are in the order of 1~10 Mpa, the fiber direction critical stress of Balsa Core is about 15 MPa.

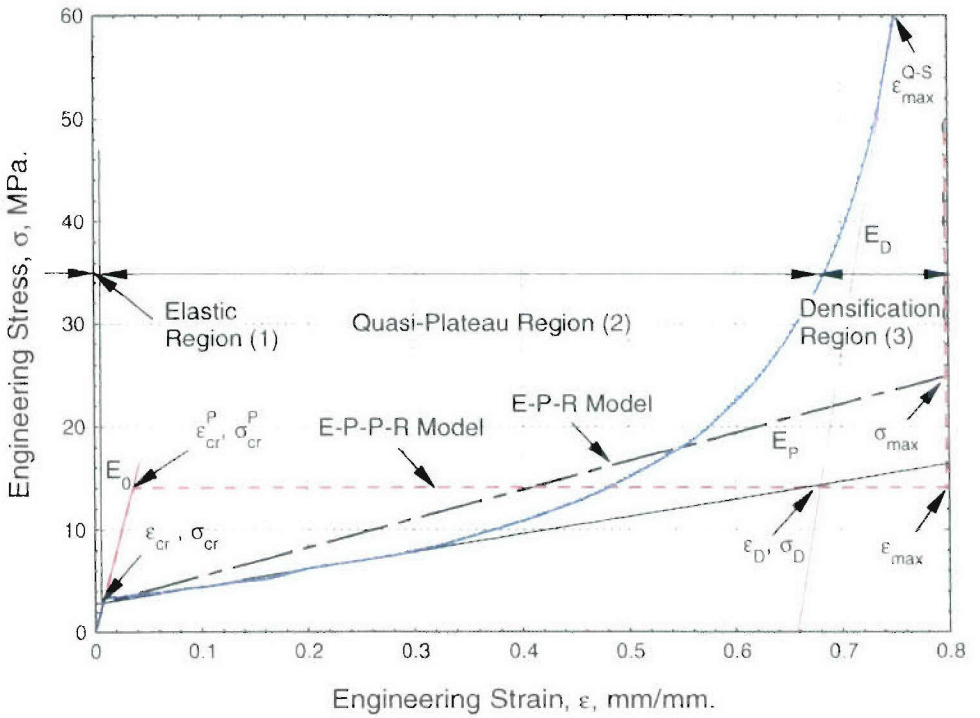

Figure 44 Axial compression behavior of cellular materials.

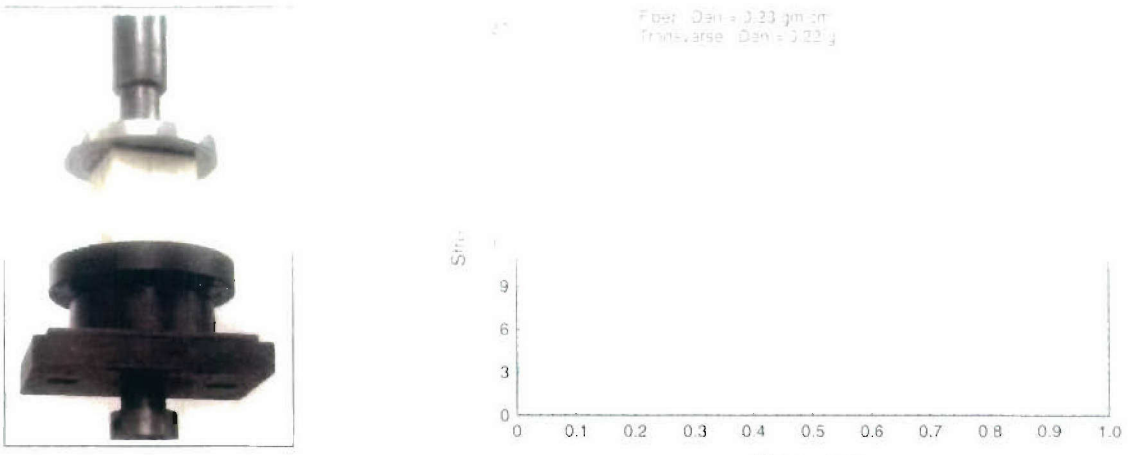

(a) Axial compression of balsa core (b) Stress-strain behavior of balsa core

Figure 45 Axial compression behavior of balsa core.

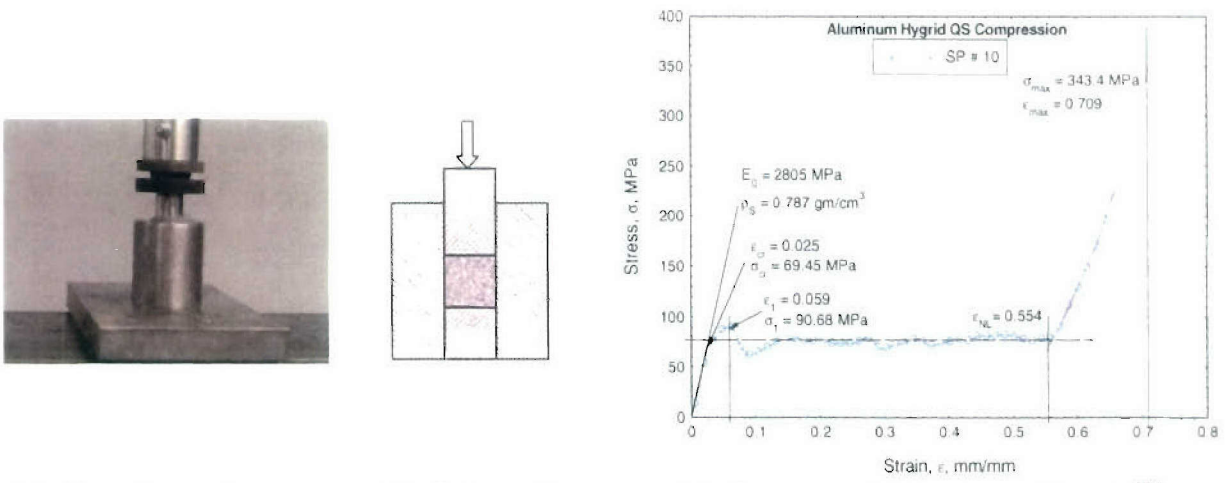

(a) Experimental set-up (b) Schematic (c) Stress-strain behavior of Hygrid™

Figure 46 Axial compression behavior of Hygrid™.

Figure 45 shows the axial compression behavior of Balsa Core material. The fiber direction behavior can be modeled as rigid-perfectly-plastic-rigid (R-P-P-R) model defined by two parameters, σ_{cr}^{R} (~15MPa) and ε_{D}^{R} (~0.6). The behavior in the transverse direction is similar to many polymeric and metal foams, i.e., non-linear with distinct zones defined as elastic, plateau, and densification regions (Figure 44).

Hygrid™ is another potential material for mine blast application. As a part of ARL-CMT program[1], the axial compression under uni-axial strain was conducted. Results show that this material has much higher critical stress (~70MPa) than Balsa Core and aluminum foam (Figure 46). Another interesting core material is WebCore, in which polymeric foam strips are filament

[1] Bazle A. Gama, Libo Ren, Adam Binkley, SM W. Islam, John W. Gillespie Jr., Quasi-Static and Dynamic Behavior of Hygrid™ aluminum Honeycomb. ARL-CMT CA9 Progress Report, October 2004.

wound with glass fiber tows and assembled together to form the core plate. Once infused with resin, parallel composite webs are formed as a repeating structure. The axial crushing behavior of this material is studied in the 3TEX SBIR N04-207 project and is shown in Figure 47. The advantage of this material is that the design can be tailored to design a core of desired critical stress.

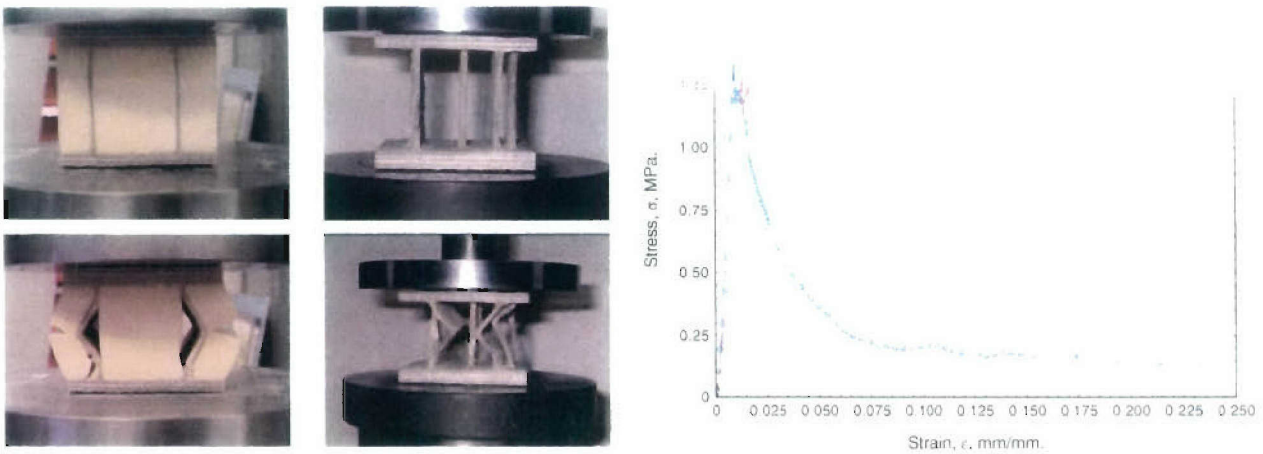

(a) With core (b) Without core (c) Engineering stress-strain

Figure 47 Axial crushing of WebCore sandwich composites.

Blast Testing of 3D Orthogonal Weave Fabric/WebCore/VE 510A-40 Sandwich Composites

Blast testing of 3D OWF/WebCore/VE 510A-40 sandwich panels was performed with a 5lb C4 explosive charge at 3-ft stand-off distance. The sandwich composite went under large deformation keeping the central core intact. The total reaction at the support is found to crush the sandwich cores. Quasi-static damage modes are found to have similar buckling stability as found under dynamic blast loading. The webs of the WebCore is found to transfer the blast momentum from the blast face to the rear face of the sandwich. Blast modeling is carried out to investigate this mechanism.

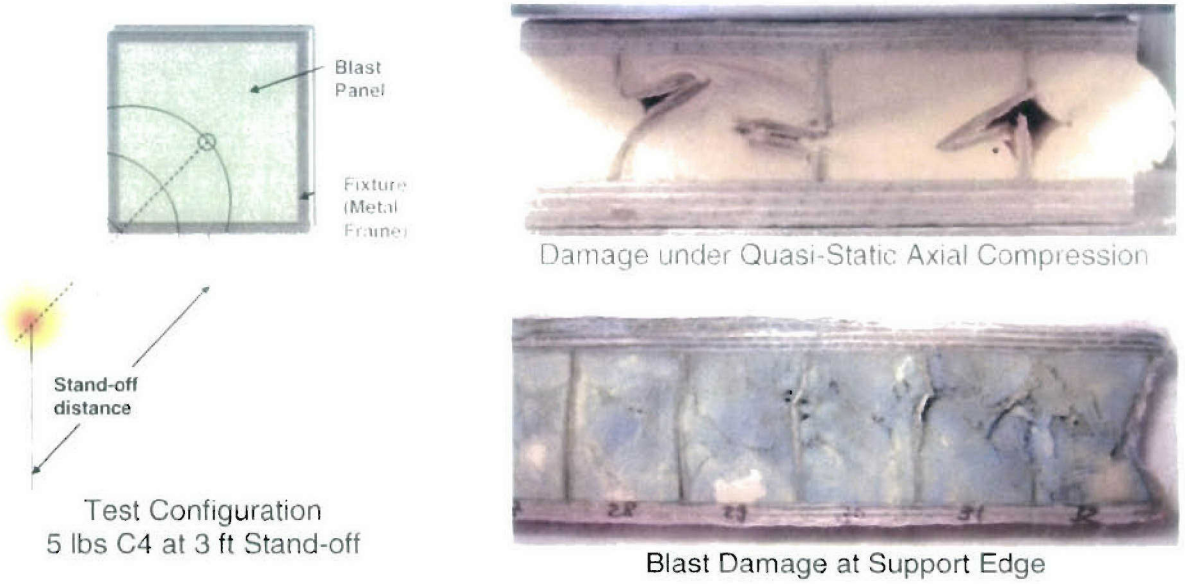

Figure 48 Blast experiments on 3D OWF/WebCore/VE 510A-40 sandwich composite.

Publications

Patents

1. Advani, S. G., M. Devillard, and J. M. Lawrence, "Molding Systems and Processes," Application filed 4 August 2005

2. Riom, N. V., M. Chohra, and S. G. Advani, "Vacuum Assisted Resin Transfer Molding Techniques," Application 60/719508 filed 22 September 09/22/2005

3. Glancey, J. L., et al., "External Vacuum Chamber for Vacuum Assisted Resin Transfer Molding," (Invention Disclosure Submitted).

4. Glancey, J. L., et al., "A Single, Multi-Section, Controllable Injection Line for Vacuum Assisted Resin Transfer Molding." (Invention Disclosure Submitted).

Journal Articles

1. Correia, N. C., F. Robitaille, A. C. Long, C. D. Rudd, P. Simacek, and S. G. Advani, "Analysis of the Vacuum Infusion Moulding Process: I. Analytical Formulation," *Composites Part A: Applied Science and Manufacturing*, v 36, n 12, p 1645-1656, December, 2005.
2. Correia, N. C., F. Robitaille, A. C. Long, C. D. Rudd, P. Simacek, and S. G. Advani, "Analysis of the Vacuum Infusion Moulding Process: I Analytical Formulation," *Composites Part A: Applied Science and Manufacturing*, **36** (12), pp. 1645-1656, 2005.
3. Devillard, M., A. Laut, and G. S. Advani, "On-Line Mixing During Injection and Simultaneous Curing in Liquid Composite Molding Processes," *Polymer Composites*, **26** (1), pp. 74-83, 2005.
4. Devillard, M., A. Laut, S. G. Advani, "On-Line Mixing During Injection and Simultaneous Curing in Liquid Composite Molding Processes," *Polymer Composites*, **26** (1), pp. 74-83, February 2005.
5. Devillard, M., K-T. Hsiao, and S. G. Advani, "Flow Sensing and Control Strategies to Address Race-Tracking Disturbances in Resin Transfer Molding – Part II: Automation and Validation," *Composites Part A: Applied Science and Manufacturing*, **36**, pp. 1581-1589, 2005.
6. Gokce, A. and S. G. Advani, "Vent Location Optimization Using Map-Based Exhaustive Search in Liquid Composite Molding Processes," *Materials and Manufacturing Processes*, **19** (3), pp.523-548, 2004.
7. Gokce, A., M. Chohra, S. G. Advani, and S. M. Walsh, "Permeability Estimation Algorithm to Simultaneously Characterize Distribution Media and Fabric Permeability Values in Vacuum Assisted Resin Transfer Molding Process," *Composites Science and Technology*, Vol 65/14, pp 2129-2139.
8. Gokce, A., M. Chohra, S. G. Advani, and S. M. Walsh, "Permeability Estimation Algorithm to Simultaneously Characterize Distribution Media and Fabric Permeability

Values in Vacuum Assisted Resin Transfer Molding Process, "*Composites Science and Technology*. **65** (14). pp. 2129-2139, 2005.

9. Lawrence, J. M. and S. G. Advani, "Dependence Map Based Flow Control to Reduce Void Content in Liquid Composite Molding," *Materials and Manufacturing Processes*, 20 (6), pp. 933-960, 2005.

10. Lawrence, J. M., J. Bau, R. Karmakar, S. G. Advani, "Characterization of Preform Permeability in the Presence of Race Tracking," *Composites Part A: Applied Science and Manufacturing*, **35**, pp. 1393-1405, 2004.

11. Lawrence, J. M., P. Fried, and S. G. Advani, "Automated Manufacturing Environment to Address Bulk Permeability Variations and Race Tracking in Resin Transfer Molding by Redirecting Flow with Auxiliary Gates," *Composites Part A: Applied Science and Manufacturing*, **36** (8), pp. 1128-1141, 2005.

12. Markicevic, B., D. Heider, S. G. Advani, and S. Walsh, "Stochastic Modeling of Preform Heterogeneity to Address Dry Spots Formation in the VARTM Process," *Composites Part A: Applied Science and Manufacturing*, **36** (6) pp. 851-858, 2005.

13. Markicevis, B., D. Litchfield, D. Heider, et al, "Role of Flow Enhancement Network during Filling of Fibrous Porous Media, *Journal of Porous Media*, **8** (3) pp. 281-297, 2005.

14. Mathieu D., K.-T. Hsiao and S. G. Advani, "Flow Sensing and Control Strategies to Address Race-Tracking Disturbances in Resin Transfer Molding —Part II: Automation and Validation," *Composites Part A: Applied Science and Manufacturing*, Available Online 18 March 2005.

15. Nalla, A., M. Fuqua, J. L. Glancey, and B. Leleiver, "A Multi-segment Injection Line and Real-Time Adaptive, Model-Based Controller for Vacuum Assisted Resin Transfer Molding," *Composites Part A: Applied Science and* Manufacturing (in review).

16. Simacek, P., and S. G. Advani, "Desirable Features in Mold Filling Simulations for Liquid Composite Molding Processes," *Polymer Composites*, Vol. 25, No. 4, pp. 355-367, August 2004.

17. Simacek, P., and S. G. Advani, "Gate Elements at Injection Locations in Numerical Simulations of Flow through Porous Media: Applications To Mold Filling," *International Journal for Numerical Methods in Engineering*, v 61, n 9, p 1501-1519, Nov 7, 2004.

18. Simacek, P., and S. G. Advani, "Simulating Three Dimensional Flow in Compression Resin Transfer Molding," *Revue Europeenne Des Elements Finis*, **14**, pp 777-802, 2005.

19. Yoon MK, Baidoo J, Gillespie JW, et al., Vacuum assisted resin transfer molding (VARTM) process incorporating gravitational effects: A closed-form solution , *journal of composite materials* 39 (24): 2227-2242 2005

20. Yoon MK, Heider D, Gillespie JW, et al., Local damage detection using the two-dimensional gapped smoothing method , *Journal Of Sound And Vibration* 279 (1-2): 119-139 Jan 6 2005.

21. Li W, Krehl J, Gillespie JW, et al., Process and performance evaluation of the vacuum-assisted process , *Journal Of Composite Materials* 38 (20): 1803-1814 2004

22. Automated VARTM processing of large-scale composite structures, *Journal Of Advanced Materials* 36 (4): 11-17 OCT 2004

23. Foley ME, Gillespie JW, Modeling the effect of fiber diameter and fiber bundle count on tow impregnation during liquid molding processes, *Journal Of Composite Materials* 39 (12): 1045-1065 JUN 2005

Conferences

1. Advani, S. G., and P. Simacek, "Recent Advances in Modeling and Simulation of Liquid Composite Molding," PPS 2005, Quebec, 2005
2. Advani, S. G., J. M. Lawrence, and P. Simacek, "Role of Flow Simulation for Design, Optimization and Control of Liquid Composite Molding Processes," ICCE 12th Conference, 2005
3. Amouroux, S. C., D. Heider, S. Lopatnikov, and J. W. Gillespie, Jr., "On the Role of Membrane to Improve Quality of VARTM-Processed Composites," ASC Conference, Drexel University, September 2005.
4. Amouroux, S. C., D. Heider, S. Lopatnikov, and J. W. Gillespie, Jr., "Membrane-Based VARTM: Membrane and Resin Interactions," SAMPE International Fall Technical Conference, Seattle, October-November 2005.
5. Gama, B. A., A. D. Bogdanovich, R. A. Coffelt, M. J. Haque, M. Rahman, and J. W. Gillespie, Jr., "Ballistic Impact Damage Modeling and Experimental Validation on a 3-D Orthogonal Weave Fabric Composite," *Proceedings of the SAMPE 2005 Symposium & Exhibition (50th ISSE)*, Long Beach, CA, May 1-5, 2005.
6. Gokce, A., A. Abu Obaid, S. Yarlagadda, and S. G. Advani, "Manufacturing and Structural Performance of Composites with Interlaminar Inserts using VARTM," *Proceedings of the SAMPE 2005 Symposium & Exhibition (50th ISSE)*, Long Beach, CA, May 1-5, 2005.
7. Gokce, A., and S. G. Advani, "Permeability Estimation Algorithm to Predict the Permeability of the Distribution Media in VARTM," *Proceedings of the SAMPE 2005 Symposium & Exhibition (50th ISSE)*, Long Beach, CA, May 1-5, 2005.
8. Lawrence, J. M., P. Hughes, and S. G. Advani, "Dependence Map Based Control of Mold Filling in Liquid Composite Molding," *Proceedings of the SAMPE 2005 Symposium & Exhibition (50th ISSE)*, Long Beach, CA, May 1-5, 2005.
9. Lawrence, J. M., P. Simacek, A. Gokce, and S. G. Advani, "Use of Flow Simulation for Design, Optimization and Control of Liquid Composite Molding Processes," ASC 2005, 2005
10. Lawrence, J. M., P. Simacek, A. Gokce, K-T. Hsiao, and S. G. Advani, "From Simulation to Production: Intelligent Manufacturing of Composite Components with Resin Transfer Molding Process," International SAMPE Technical Conference, SAMPE 2004, 2004, p 483-495.
11. Nalla, A. and J.L. Glancey. 2005. Closed Loop Control of Resin Flow in VARTM using a Multi-segment Injection Line and Real-Time Adaptive, Model-Based Control. Paper No. IMECE2005-81767. Proceedings of the 2005 ASME International Annual Meeting, Orlando, FL.

12. Neacsu, V., A. Abu Obaid, and S. G. Advani, "Role of Capillarity in Fiber Tow Impregnation During Composites Processing" *Proceedings of the SAMPE 2005 Symposium & Exhibition (50th ISSE)*, Long Beach, CA, May 1-5, 2005.

13. Simacek, P., A. Gokce, J. M. Lawrence, and S. G. Advani, "Numerical Modeling of Mold Filling in Liquid Composites Molding: Novel Issues in Well Established Field," CANCOM 2005, Vancouver, 2005.

14. Ali Gokce, Pavel Simacek, Hope Deffor, Suresh Advani, Dirk Heider Center for Composite Materials, University of DE, Newark, DE 19716 David B Powell, Jacob Alexander Triton Systems, Inc., 200 Turnpike Road, Chelmsford, MA 0182, RISK REDUCTION VIA VIRTUAL FLOW SIMULATION IN MANUFACTURING OF SANDWICH PANELS USING VARTM PROCESS

15.

Theses and Dissertations

1. Kasprzak, S. 2005, Honors Degree with Distinction in Mechanical Engineering Thesis, VARTM Flow Modification with Machine Vision and Robotic Control, Newark, DE

2. Nalla, A. 2005, Masters in Mechanical Engineering Thesis, Modeling and Adaptive Control of Vacuum Assisted Resin Transfer Molding Systems with Segmented Injection and Vacuum Lines., Newark, DE

3. 28. Mourad Chohra (2005), "Modeling of Filtration Process during Manufacturing of Functionally Graded Composites with Particulate Suspensions"

4. Jeff Lawrence, Ph.D. (2005), "Methodologies for Resin Flow Prediction and Manipulationin Liquid Composite Molding Processes"